`LC-PLM`: **Long-context Protein Language Modeling Using Bidirectional Mamba with Shared Projection Layers**

Yingheng Wang[*]   *yw2349@cornell.edu*
Department of Computer Science
Cornell University

Zichen Wang[†]   *zichewan@amazon.com*
Amazon

Gil Sadeh   *gilsadeh@amazon.com*
Amazon

Luca Zancato   *zancato@amazon.com*
Amazon

Alessandro Achille   *aachille@amazon.com*
Amazon

George Karypis   *gkarypis@amazon.com*
Amazon

Huzefa Rangwala[‡]   *rhuzefa@amazon.com*
Amazon

Abstract

Self-supervised training of language models (LMs) has seen great success for protein sequences in learning meaningful representations and for generative drug design. Most protein LMs are based on the Transformer architecture trained on individual proteins with short context lengths. Such protein LMs cannot extrapolate to longer proteins and protein complexes well. They also fail to account for the underlying biological mechanisms carried out by biomolecular interactions and dynamics i.e., proteins often interact with other proteins, molecules, and pathways in complex biological systems. In this work, we propose `LC-PLM` based on an alternative protein LM architecture, `BiMamba-S`, built upon selective structured state-space models, to learn high-quality universal protein representations at the amino acid token level using masked language modeling. We also introduce its graph-contextual variant, `LC-PLM-G`, which contextualizes protein-protein interaction (PPI) graphs for a second stage of training. `LC-PLM` demonstrates favorable neural scaling laws, better length extrapolation capability, and up to 30% and 16% improvements on protein downstream tasks compared to Transformer-based ESM-2 when trained with 100B and 1T tokens, respectively. `LC-PLM-G` further trained within the context of PPI graphs shows promising results on protein structure and function prediction tasks. Our study demonstrates the benefit of increasing the context size with computationally efficient LM architecture (e.g., structured state space models) in learning universal protein representations and incorporating molecular interaction contexts contained in biological graphs.

---

[*]This work was completed while the author was an intern at Amazon.

[†]Corresponding author.

[‡]Huzefa Rangwala is on LOA as a Professor of Computer Science at George Mason University. This paper describes work performed at Amazon.

1 Introduction

Most biological sequences are derived from genomes, which are long DNA sequences: human chromosomes range from 50 to 300 million base pairs. The protein-coding regions, which can be considered as the translated substrings of the genome, are relatively shorter (the majority are < 3,000 amino acids), albeit with a few exceptions, such as Titin, composed of 34K amino acids. The prevalent protein language models (pLMs), e.g. ESM-2 (Lin et al., 2023), choose 1024 as the context length as it fits 97.4% of proteins. However, it does not natively support tasks that require long-range context windows to reason over multiple related sequences, such as genomic interactions, protein-protein interactions (PPI), protein function prediction, and 3D structure prediction of long proteins and protein complexes. Another challenge for modeling long-range biological contexts lies in their non-sequential nature. For instance, the useful context for genomic interactions and PPIs often span across regions from different chromosomes, and capturing information within an LM of such interactions usually requires biomedical knowledge graphs for good performance on these tasks (Kovács et al., 2019; Sousa et al., 2024).

Large LMs including those trained on protein sequences, are predominantly based on the Transformer (Vaswani et al., 2017) with multi-head attention. Despite its state-of-the-art performance on virtually all types of data modalities (texts, vision, audio, etc.), it suffers from quadratic time and space complexity due to the lengths of the input sequences. Additionally, transformer models are known to have poor length extrapolation quality and do not achieve the same level of performance when evaluated on sequences longer than seen during pretraining. Recent work in alternative architectures such as convolutional (e.g. Hyena (Poli et al., 2023)) and selective structured state space models (SSMs) (e.g. Mamba (Gu & Dao, 2024)) have demonstrated competitive performance and preferable scaling properties on long context compared to Transformers and extensions including linear attention approximation variants (Katharopoulos et al., 2020; Zhai et al., 2021; Peng et al., 2023). Although recent studies have leveraged these novel architectures to train LMs for DNA sequences (Nguyen et al., 2024b;a; Schiff et al., 2024), studies examining their feasibility as protein LMs are limited. There is also a research gap on how to effectively leverage the long-context capability of these architectures to model graphs of sequences i.e., how to leverage PPI graphs to improve LM's ability to reason across interacting (related) proteins.

In this work, we explore alternative architectures based on Mamba to improve the long-context capability of pLMs. We train a long-context pLM (`LC-PLM`) using bidirectional Mamba with shared projection layers (`BiMamba-S`) on protein sequences from `UniRef50` with masked language modeling (MLM) objective. Results show favorable neural scaling laws, length extrapolation properties on `UniRef90`, and better downstream task performance on `TAPE` (Rao et al., 2019) and `ProteinGym` (Notin et al., 2024) than its Transformer counterpart, namely ESM-2. Such long-context and length ex-
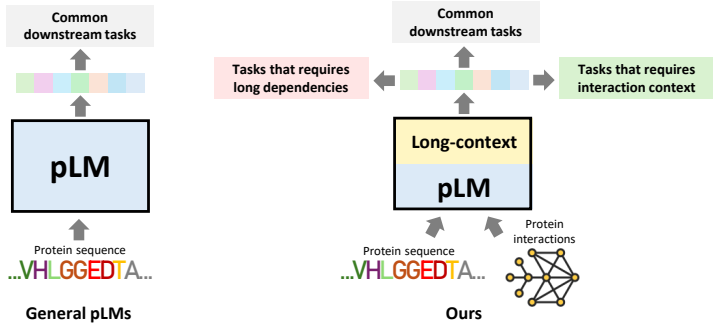

Figure 1: Our model enables long-context capability, length extrapolation ability, better neural scaling law, and interaction context-aware inference.

trapolation properties facilitate and improve structure prediction of long proteins and protein complexes from `CASP14`, `CASP15-multimers`, and `Benchmark2`. Next, we train a graph-contextualized variant `LC-PLM-G`, which uses a proposed novel second-stage training strategy to leverage the long-context capabilities of `BiMamba-S` to encode useful information from interaction graphs (e.g., PPI). Trained on sampled random walks that are composed of sequences of proteins, `LC-PLM-G` improves performance on remote homology prediction, node-level protein function prediction (`ogbn-proteins`), and link-level PPI prediction (`ogbl-ppa`) (Hu et al., 2020). Our contributions can be summarized into three folds as follows:

- We develop a long-context pLM (`LC-PLM`) with an alternative architecture based on a more sample & compute-efficient bidirectional Mamba architecture with shared projection layers (`BiMamba-S`) pretrained on `UniRef50` with MLM objective.

- We demonstrate that `LC-PLM` has improved length extrapolation capabilities and favorable scaling laws, and outperforms ESM-2 by up to 30% and 16% on various downstream tasks (e.g. protein structure prediction (`CASP15-multimers`, `CASP14`, `Benchmark2`), tasks in `TAPE` and `ProteinGym`) when trained with 100B and 1T tokens, respectively.

- To encode biological interaction information, we propose a novel second-stage training based on random walks on graphs to extend the long-context capabilities of `LC-PLM` that leverages the PPI graph context. We demonstrate its effectiveness in capturing graph-contextual information on predicting remote homology (`TAPE`), protein functions (`ogbn-proteins`), and PPI links (`ogbl-ppa`).

2 Related Works

2.1 Long-context LMs and State Space Models

Since their introduction, Transformers (Vaswani et al., 2017) with multi-head attention have been successfully applied in many different applications in natural language and computer vision. However, while being relatively straightforward to scale the number of parameters, Transformer models have a quadratic dependence on the context length during training and are linear at inference time, making them expensive to scale to long context. Alternative to Transformers, Recurrent Neural Networks (RNNs) (Hochreiter, 1991; Bengio et al., 1994; Hochreiter & Schmidhuber, 1997) scale more favorably with context length and have linear dependency at training time and constant at inference time. However, generic non-linear RNNs cannot be parallelized on modern hardware due to the sequential nature of their gradient update rule (Bengio et al., 1994).

To improve RNNs scalability on modern hardware, recent works on SSMs (Gu et al., 2021; Fu et al., 2022; Gu & Dao, 2024) propose to linearize RNNs dynamics and use efficient hardware-aware algorithms. A notable example is Mamba (Gu & Dao, 2024), which leverages the associative scan to efficiently process arbitrarily long sequences in linear time, and Mamba-2 (Dao & Gu, 2024) that greatly improves over Mamba by implementing SSM layers using structured matrix multiplications to better leverage modern Tensor cores.

To further harvest the benefits of SSM and Transformer primitives, hybrid models have been proposed in Zancato et al. (2024); Lieber et al. (2024); Arora et al. (2024); De et al. (2024); Botev et al. (2024); Waleffe et al. (2024). There are also efforts trying to extend Mamba models to graph data (Wang et al., 2024; Behrouz & Hashemi, 2024). However, unlike our `LC-PLM-G`, which learns token-level protein representations within graph context from the graph of sequences, they focus on learning node/graph-level representations that only work for generic graph tasks where nodes do not contain sequences (see Table 1)[1].

Method	Universality	Fine granularity	Long-context capability *Handleability* & *Performance*		Graph context	Large-scale model
ProtGPT (2022)	✓	✓	✗	✗	✗	✗
ESM-2 (2023)	✓	✓	✗	✗	✗	✓
CARP (2024)	✓	✓	✓	✗	✗	✓
ProtHyena (2024)	✓	✓	✓	✗	✗	✗
PoET (2024)	✗	✓	✗	✗	✗	✗
ProtMamba (2024)	✗	✓	✗[2]	✗	✗	✗
PTM-Mamba (2024)	✗	✓	✓	–	✗	✓
Graph-Mamba (2024)	✗	✗	✓	–	✓	✗
GMN (2024)	✗	✗	✓	–	✓	✗
`LC-PLM`	✓	✓	✓	✓	✗	✓
`LC-PLM-G`	✓	✓	✓	✓	✓	✓

Table 1: Comparison of `LC-PLM` and `LC-PLM-G` to other protein LMs and graph SSMs in terms of enabling universal representations, AA token-level fine granularity, long-context capability, graph contextual information, large model size, and a large number of pretrained tokens.

---

[1]We provide the concrete definitions in Appendix A for all criterions used in Table 1.

2.2 Long-context LMs for biological sequences

To model the long-range interactions without sacrificing single nucleotide level resolution, long-context capable LM architectures have been developed for DNA sequences, including HyenaDNA (Nguyen et al., 2024b), Evo (Nguyen et al., 2024a), and Caduceus (Schiff et al., 2024). These studies have shown that alternative architectures based on SSMs exhibit better scaling laws than Transformers on genomic data and DNA-specific tasks. Protein sequence LMs with alternative architectures have also been explored to improve computational efficiency and enable the modeling of longer protein sequences. For instance, CARP (Yang et al., 2024) is a protein LM with dilated convolution layers. Pretrained with MLM objective, CARP achieved comparable pretraining scaling properties with its Transformer counterpart ESM-1b (Rives et al., 2021) and scales better on long sequences. ProtHyena (Zhang, 2024) is a small 1.6M parameter decoder-only LM based on the Hyena operator pretrained on protein sequences and has demonstrated some improvement over ProtGPT (Ferruz et al., 2022) with comparable model sizes.

Some works exploit the long-context capability of LMs to model sets of homologous protein sequences such as those in multiple sequence alignment (MSA), which further organize a set of protein sequences by aligning evolutionary conserved amino acids across the set of sequences. PoET (Truong Jr & Bepler, 2024) proposed a tiered variant of Transformer to model the invariant relationships between multiple protein sequences from MSAs, whereas ProtMamba (Sgarbossa et al., 2024) trains a Mamba-based protein LM using concatenated sequences from MSAs with causal language modeling and infilling objective. PTM-Mamba (Peng et al., 2024) addresses post-translational modifications (PTM) of protein sequences introducing PTM tokens to amino acid tokens and subsequently trains a bidirectional Mamba model with these PTM tokens. We provide additional discussion on other pLMs and related variants in Appendix B.

Instead of training protein sequences from very specific types of data like MSAs or PTMs, we emphasize that **our work** focuses on long-context modeling of individual protein sequences and related protein sequences within biomedical graphs, which learns universal AA token-level protein representations that are more generalizable and can encode information from biological interactions (see Table 1 for a detailed comparison).

2.3 Protein LMs trained on graphs

Graphs are ubiquitous in biomedical domains as they are suitable for organizing and representing complex biological systems, such as gene regulatory networks and PPI graphs (Wang et al., 2022). The relationships among proteins embedded in biomedical graphs have also been used to train pLMs. The common strategies for incorporating graph information include pretraining LMs with graph-specific objectives in addition to self-supervised LM objectives. The graph-specific objective can be link-prediction on homogeneous graphs (Yasunaga et al., 2022; McDermott et al., 2023), knowledge graph embedding (KGE) objectives (Zhang et al., 2022) or contrastive loss (Wang et al., 2023) on heterogeneous graphs. One limitation of such approaches is the inability to jointly model the implicit token-wise interactions beyond a pair of sequences. After all, link-prediction and KGE only take two sequences as input. In our work, we use homogeneous PPI graphs and exploit the long-context capability of SSM-based LM to model token-wise interactions beyond two sequences.

3 Preliminaries

Structured State Space Models Modern Structured SSMs are derived from first-order differential equations that map the input sequence $x(t)$ to the output sequence $y(t)$ through hidden state $h(t)$:

$$\mathbf{h}'(t) = \mathbf{A}\mathbf{h}(t) + \mathbf{B}x(t), \quad y(t) = \mathbf{C}\mathbf{h}(t) \tag{1}$$

where $\mathbf{A} \in \mathbb{R}^{N \times N}$, $\mathbf{B} \in \mathbb{R}^{N \times D}$ and $\mathbf{C} \in \mathbb{R}^{D \times N}$. The variables N and D refer to the state dimension and the (expanded) input dimension respectively. The continuous dynamical system characterized by $\mathbf{A}$, $\mathbf{B}$ can be discretized to $\bar{\mathbf{A}}, \bar{\mathbf{B}}$ by zero-order holding and time sampling at intervals of Δ, defined as follows:

$$\bar{\mathbf{A}} = \exp(\Delta\mathbf{A}), \quad \bar{\mathbf{B}} = (\Delta\mathbf{A})^{-1}(\exp(\Delta\mathbf{A}) - \mathbf{I}) \cdot \Delta\mathbf{B}. \tag{2}$$

---

[2]ProtMamba used an unextrapolatable learnable positional encoding that sacrificed the long-context capability of Mamba. We discuss more in Appendix A.

The formula of a discretized SSM can then be written as:

$$\mathbf{h}_k = \bar{\mathbf{A}}\mathbf{h}_{k-1} + \bar{\mathbf{B}}x_k, \quad y_k = \mathbf{C}\mathbf{h}_k \tag{3}$$

The main benefit of discretized SSMs (Gu et al., 2021) over their continuous counterpart is that they can be trained efficiently using their parallel convolutional representation and can be efficiently deployed at inference time with their recurrent form. However, the ability to model long-range interactions of SSMs is limited by the impulse response of the discrete dynamical system they implement, the S4 model (Gu et al., 2020; 2021) mitigates such limitation by introducing the HIPPO Matrix to the initialization of $\mathbf{A}$.

Selection Mechanism and Mamba   The main limitation of the SSMs described so far is that they cannot model complex input-varying interactions across the sequence dimension. Thus, Mamba (Gu & Dao, 2024) parameterizes the matrices $\mathbf{B}$, $\mathbf{C}$ and Δ in an input-dependent (data-driven) manner, introducing a selection mechanism into the S4 model. However, introducing such data dependency makes the parallelizable convolutional representation unfeasible, hence, Mamba uses a novel hardware-aware parallel computing algorithm (based on the associative scan) to ensure the efficient training of the model and leading to linear computational complexity and outstanding capabilities in modeling long-term dependencies. A Mamba model (*selective* SSM) that enables dependence of the parameters $\mathbf{B}$, $\mathbf{C}$ and Δ on the input x_t can be formulated as:

$$\mathbf{B}_t = \text{Linear}_{\mathbf{B}}(x_t) \quad \mathbf{C}_t = \text{Linear}_{\mathbf{C}}(x_t) \tag{4}$$
$$\Delta_t = \text{softplus}(\text{Linear}_{\Delta}(x_t)), \tag{5}$$

where $\text{Linear}(\cdot)$ represents a linear projection and $\text{softplus}(\cdot) = \log(1 + \exp(\cdot))$.

4   `LC-PLM`: **Long Context Protein Language Model**

In this section, we first introduce the design choice of using bidirectional Mamba (`BiMamba`) with shared projection layers (`BiMamba-S`) for building up the model architecture of `LC-PLM`, and then we discuss how we develop the two-stage training recipe to obtain high-quality universal protein representations using MLM and encode biologically meaningful interaction information with a novel graph context-aware training approach.

4.1   `BiMamba-S`: **Bidirectional Mamba with Shared Projection Layers**

`BiMamba` is an extension from standard Mamba block and has been applied in various domains, e.g. time-series forecasting (Liang et al., 2024), audio representation learning (Erol et al., 2024), visual representation learning (Zhu et al., 2024), DNA modeling (Schiff et al., 2024), and graph learning (Behrouz & Hashemi, 2024). The following reasons suggest we consider `BiMamba` as the design choice: (i) Mamba is good at *capturing long-range dependencies* and *extrapolating on longer sequences*, which benefit a lot of downstream tasks on protein complexes and PPI graphs. (ii) standard Mamba only does unidirectional (associative) scans for causal sequence modeling. To *perform MLM to learn high-quality universal protein representations*, we introduce a modified bidirectional scan to capture information from both ends.

In general, the l-th `BiMamba` block takes in an input sequence of tokens $\mathbf{T}_{l-1} \in \mathbb{R}^{B \times S \times D}$ and output $\mathbf{T}_l \in \mathbb{R}^{B \times S \times D}$ where B, S, D represent the batch size, the input dimension, and the hidden state dimension. Then a residual connection adds the input and output together to get $\mathbf{T}_l$. After going through $L\times$ `BiMamba` blocks, the output $\mathbf{T}_L$ will be normalized first and then fed into a prediction head to get final scores. This procedure can be formulated as follows:

$$\mathbf{T}_l = \text{BiMamba}\left(\mathbf{T}_{l-1}\right) + \mathbf{T}_{l-1} \tag{6}$$
$$\hat{p} = \text{PredictionHead}\left(\text{Norm}\left(\mathbf{T}_L\right)\right) \tag{7}$$

Specifically, in one `BiMamba` block, the input sequence $\mathbf{T}_{l-1}$ and the flipped $\hat{\mathbf{T}}_{l-1}$ will be first normalized and then linearly projected to $\mathbf{X}_{l-1} \in \mathbb{R}^{B \times S \times E}$ and $\mathbf{Z}_{l-1} \in \mathbb{R}^{B \times S \times E}$. $\mathbf{X}_{l-1}$ and the flipped $\hat{\mathbf{X}}_{l-1}$ will be fed into the forward and inverse Mamba block respectively for a bidirectional scan. In each Mamba block, $\mathbf{X}_{l-1}$

and $\hat{\mathbf{X}}_{l-1}$ will be first passed through a 1-D convolution layer and a SiLU activation (Nwankpa et al., 2018), and then linearly projected to $\mathbf{B}_{l-1} \in \mathbb{R}^{B \times S \times N}, \mathbf{C}_{l-1} \in \mathbb{R}^{B \times S \times N}, \Delta_{l-1} \in \mathbb{R}^{B \times S \times E}$ and $\hat{\mathbf{B}}_{l-1}, \hat{\mathbf{C}}_{l-1}, \hat{\Delta}_{l-1}$, where Δ_{l-1} and $\hat{\Delta}_{l-1}$ transform $\mathbf{A}_{l-1}, \mathbf{B}_{l-1}$ and $\hat{\mathbf{A}}_{l-1}, \hat{\mathbf{B}}_{l-1}$ to $\bar{\mathbf{A}}_{l-1} \in \mathbb{R}^{B \times S \times E \times N}, \bar{\mathbf{B}}_{l-1} \in \mathbb{R}^{B \times S \times E \times N}$ and $\hat{\bar{\mathbf{A}}}_{l-1}, \hat{\bar{\mathbf{B}}}_{l-1}$. A standard SSM block will be then applied to obtain $\mathbf{Y}_{l-1} \in \mathbb{R}^{B \times S \times E}$ and $\hat{\mathbf{Y}}_{l-1}$, which later will be gated by $\mathbf{Z}_{l-1}$ and added together to get the candidate output. Lastly, a residual connection will be applied on a linear projection of the candidate output and input sequence $\mathbf{T}_{l-1}$ to get the final output $\mathbf{T}_l$. We provide an algorithmic block and a detailed breakdown to describe this computation process in Appendix J.

Shared Projection Layers To explore a more efficient implementation of `BiMamba`, we propose to use the shared linear projection layers for the forward input $\mathbf{T}_{l-1}$ and the flipped $\hat{\mathbf{T}}_{l-1}$. This design choice helps make the entire model $2\times$ deeper with almost the same parameter counts (Schiff et al., 2024). We refer to this building block as `BiMamba-S` (illustrated in Figure 2). Note that this is different from the inner BiMamba block used in Zhang et al. (2024a); Zhu et al. (2024), where they just flipped the linearly projected hidden states. We also find that, empirically, the deeper model using `BiMamba-S` shows superiority in terms of sample & compute efficiency (4.5% improvement on evaluation loss) and performance gain on downstream tasks (an average of 4.1% improvement on TM score of structure prediction) as we expected. More results and details are shown in Section 5.3.

Untied Input & Output Embeddings Notably, we opt to use untied input and output embeddings for the `BiMamba-S` encoder. Empirically we find that untied embeddings yield better evaluation loss during MLM training compared to tied embeddings, despite the latter being the standard practice. This finding aligns with previous research (Gao et al., 2019; Ethayarajh, 2019), which highlights that tying input and output embeddings leads to *anisotropic* word embeddings in contextualized pretrained models, significantly constraining their expressiveness.

4.2 Two-stage Training Recipe

Our training procedure can be decomposed into two stages: (i) long-context protein language modeling and (ii) protein language modeling within graph contexts. The first stage will enforce `LC-PLM` to learn the universal token-level representations of individual proteins and the second stage will put the protein sequences into the related graph contexts and `LC-PLM-G` will learn to capture biologically meaningful interaction information.
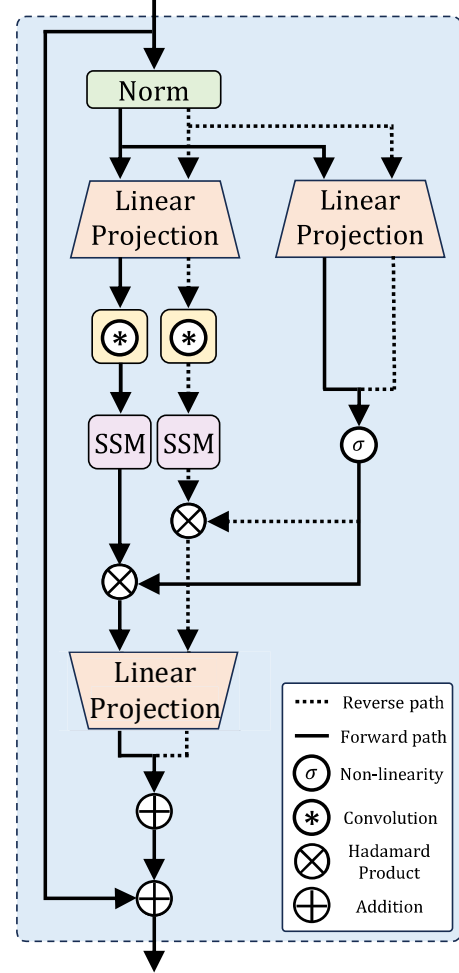

Figure 2: `BiMamba-S` block. The forward and reverse modules share the linear projection layers. The normalized input will be reversed along the sequence dimension before being fed in. The output of the reversed will be flipped back and then added to the forward's output.
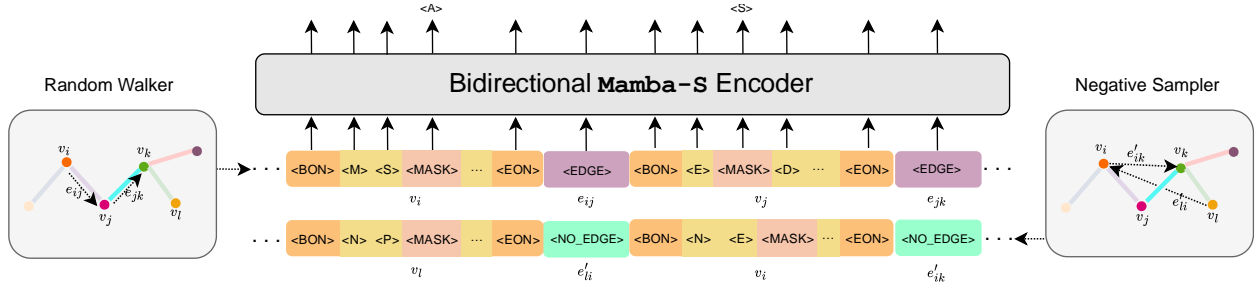
Long-context Protein Language Modeling `LC-PLM` is trained with `BiMamba-S` on individual protein sequences where it can leverage the power of SSM modules to effectively capture long-range dependencies within sequences. Specifically, treating the protein sequences as a collection of amino acid (AA) tokens, the model learns fine granular and universal token-level representations using MLM, which can be generalized across different types of protein sequences. For the masking strategy, we follow BERT (Devlin, 2018) in which 15% of AA tokens in a protein sequence will be "masked". Of the 'masked' tokens, 80% are replaced with `[MASK]`, 10% are replaced with a random token from the vocabulary, and 10% are left unchanged.

Figure 3: The illustration of graph-contextual protein language modeling (`LC-PLM-G`). The positive paths are sampled with random walks on the graph and the same number of negative paths are sampled from disconnected node pairs randomly. The sampled paths will be transformed into multi-protein sequences composed of AA tokens and special graph identifier tokens. The `BiMamba-S` encoder is trained using MLM, the same as in the first-stage training.

Graph-contextual Protein Language Modeling To encode biologically meaningful interaction information into protein representations, we propose the second-stage training within a graph context where a node represents an individual protein sequence and an edge indicates the existence of PPI. We refer to this graph-contextually trained model variant as `LC-PLM-G`. Wang et al. (2022) and Behrouz & Hashemi (2024) propose to tokenize the graph into either flattened node sequences with prioritization strategy (e.g., node degree) or induced subgraphs. However, the former discards the graph topology information and the latter provides only 2-D tokens that cannot be used as the input of language models. Therefore, we propose to construct the graph-contextual input via random walks (Perozzi et al., 2014; Grover & Leskovec, 2016), which can both effectively capture the graph topology and provide 1-D sequences. Consider an undirected, unweighted, PPI graph $\mathcal{G} = (V, E)$. Formally, a random walk of length l can be simulated by

$$P(n_i = v \mid n_{i-1} = u) = \begin{cases} \frac{\pi_{uv}}{Z} & \text{if } (v, u) \in E \\ 0 & \text{otherwise} \end{cases} \tag{8}$$

where n_i denotes the ith node in the walk, π_{uv} is the unnormalized transition probability between nodes (u, v), and Z is the normalizing constant. We also set two parameters p and q as in Grover & Leskovec (2016) to interpolate the behavior of random walker in between breath-first and depth-first search (see Appendix K). Then, the nodes in each random walk will be expanded as a sequence of proteins composed of AA tokens. We also sample a sequence of disconnected nodes of the same length l as the negative paths.

Although this gives us a principled way to form input multi-protein sequences for language models within graph context, the input still needs special identifiers to let the language model precept the graph topological information and be aware of which protein each AA token belongs to. Thus, we design four new tokens (`[BON]`, `[EON]`, `[EDGE]`, `[NO_EDGE]`) to help encode such graph context information, where the first two indicate the begin and end of a node and the last two represent if there exists an edge. We provide a visual illustration of this graph-contextual training regime in Figure 3.

5 Experiments

We conduct experiments to evaluate the effectiveness of `LC-PLM` and `LC-PLM-G` and their building block `BiMamba-S`. We will address the following research questions. **(RQ1)** What is the scaling behavior of `LC-PLM`? How does it compare with its Transformer-based counterpart ESM-2? **(RQ2)** Does `LC-PLM` show stronger length extrapolation capability than ESM-2? **(RQ3)** Will `BiMamba-S` architecture be more effective in long-context protein language modeling? **(RQ4)** Does long-range dependencies help with protein structure prediction? **(RQ5)** Does `LC-PLM-G` learn graph-contextual (relational) information? **(RQ6)** Does `LC-PLM-G` with biological interaction information learned in the second-stage training help with common downstream tasks? **(RQ7)** Does `LC-PLM-G` improve protein function prediction and link prediction on the PPI graph? We provide the experimental setup, dataset description, and task definition in Appendices C and D.
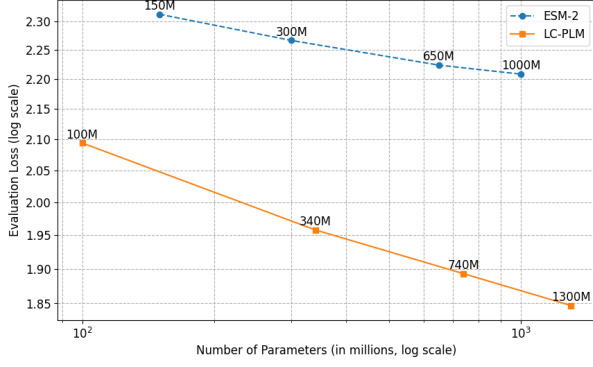
Figure 4: Evaluation loss across different model sizes for `LC-PLM` and ESM-2, showing that `LC-PLM` has a better scaling behavior when increasing the number of model parameters.
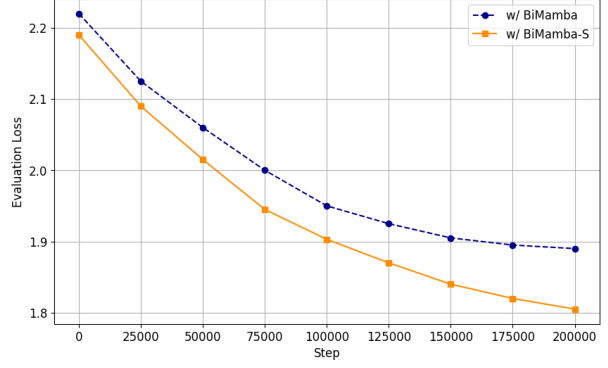

Figure 5: Evaluation loss comparison between `BiMamba` and `BiMamba-S` over training steps.

5.1 (RQ1) Exploring the Scaling Law

We train `LC-PLM` on 20B `UniRef90` sequences and evaluate it on a held-out set of 250K `UniRef90` sequences. We test four different model sizes for both `LC-PLM` and ESM-2. The model sizes for `LC-PLM` are 100M, 340M, 740M, and 1.3B parameters to accommodate `BiMamba-S` architecture, while for ESM-2, they are 150M, 300M, 650M, and 1B. The results demonstrated that `LC-PLM` not only achieved better evaluation loss (average cross-entropy across all tokens) with a similar model size (with an average of 13.5% improvement) compared to ESM-2 but also exhibited superior scaling behavior (sharper slope) when increasing the model size, as shown in Figure 4. This aligns with the discovery in Gu & Dao (2024) that Mamba has better neural scaling law compared to Transformers in language modeling. This may also be due to the useful long-range dependencies in protein sequences captured by `LC-PLM` and the deeper architecture achieved with `BiMamba-S`.

5.2 (RQ2) Length Extrapolation Evaluation

We split the UniRef90 sequences into 7 bins w.r.t. the sequence length (i.e. 0-128, 128-256, 256-512, 512-1024, 1024-2048, 2048-4096, and 4096-8192). We train three sizes of `LC-PLM` (100M, 340M, 740M) and ESM-2 (150M, 300M, 650M) on the bin of 128-256 and then evaluate them on all bins (including a held-out set of 128-256). Our findings show that `LC-PLM` maintains low evaluation loss across sequence lengths, while ESM-2 struggles with both shorter and longer sequences, especially when the lengths are underrepresented in the training set. This concludes that `LC-PLM` can extrapolate better with length due to the stronger length extrapolation capability of `BiMamba-S` (Gu & Dao, 2024) compared to ESM-2, which uses RoPE (Su et al., 2024)
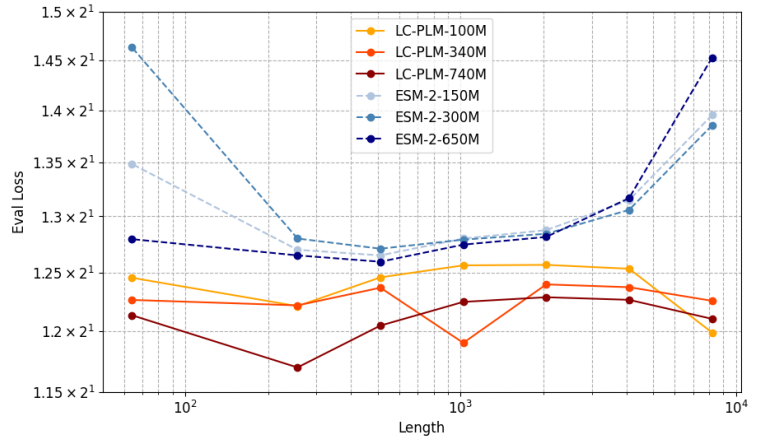

Figure 6: Length extrapolation results comparing `LC-PLM` versus ESM-2 on evaluation loss across different sequence lengths. `LC-PLM` can achieve consistent performance when extrapolating on longer sequences.

to extend context beyond pretraining. The results are shown in Figure 6.

5.3 (RQ3) The Effectiveness of `BiMamba-S`

Using shared linear projection layers in `BiMamba-S` allows for $2\times$ deeper models with similar parameter counts. In our analysis, we compare the evaluation loss of our 740M model with `BiMamba-S` and its `BiMamba` counterpart that halves the depth. The training set is `UniRef50` and the evaluation set is a held-out set of 250K `UniRef90` sequences, the same as in the scaling law experiments. Our results show that this parameter-efficient approach to increasing the model depth effectively improves evaluation loss by 4.5%, as shown in Figure 5. We also verify the effectiveness of `BiMamba-S` on structure prediction in Table 2, where the deeper model improves by 6.7% on `CASP15-multimers`, 4.6% on `CASP14`, and 1.5% on `Benchmark2`. This empirical evidence matches the theory that more hidden layers in deep neural networks can be benefited from more representation power gain, proposed in (Telgarsky, 2016). This also suggests a potentially better scaling strategy for training pLMs with the fixed parameter count, i.e. stacking more layers instead of having more hidden units.

5.4 (RQ4) Protein Structure Prediction with LMFold

We also evaluate `LC-PLM`'s ability to predict protein's 3-D structures. It has been shown that protein LMs capture various levels of protein structure information (Rives et al., 2021; Rao et al., 2020; Lin et al., 2023), despite being trained on primary sequences alone. Inspired by the ESMFold (Lin et al., 2023) architecture, which uses the residue-level embeddings and, optionally, attention maps as features to predict the 3-D structures directly without MSA[3], we developed a protein folding model named LMFold, which generalizes ESMFold's Folding Trunk and Structure Module to work with protein LMs with decoder-only and encoder-decoder architectures. Briefly, LMFold takes the residue-level embeddings for a given protein sequence as features to predict the all-atom coordinates of the protein structure. To further simplify LMFold, we only use 1 folding block of the structure module. Note that the goal of this task is not to develop the state-of-the-art protein folding model, but rather to quantify the potential of pretrained protein LMs for their learned structural information. To train LMFold, we use the *Frame Aligned Point Error (FAPE)* and *distogram* losses introduced in AlphaFold2 (Jumper et al., 2021), as well as heads for predicting *LDDT* and the *pTM score*. We weigh these 4 loss terms using the default constants proposed in OpenFold (Ahdritz et al., 2024).

Model (#Tokens trained)	CASP15-multimers	CASP14	Benchmark2
ESM-2-650M (100B)	0.3992 ± 0.0418	0.3403 ± 0.0527	0.4724 ± 0.0407
`LC-PLM`-740M w/ `BiMamba` (100B)	0.4538 ± 0.0151	0.3827 ± 0.0124	0.6012 ± 0.0101
`LC-PLM`-740M w/ `BiMamba-S` (100B)	0.5012 ± 0.01870	0.4014 ± 0.0190	0.6128 ± 0.0117
ProtMamba-public[4]	0.3561 ± 0.0250	0.3176 ± 0.0219	0.4431 ± 0.0224
ESM-2-650M-public (1T)[5]	0.4750 ± 0.0120	0.4300 ± 0.0179	0.6491 ± 0.0162
`LC-PLM`-740M (1T)	$\mathbf{0.5515 \pm 0.0254}$	$\mathbf{0.4650 \pm 0.0215}$	$\mathbf{0.7075 \pm 0.0248}$

Table 2: Structure prediction performance (*TM score*) on `CASP15-multimers`, `CASP14`, and `Benchmark2`. We perform 3 runs using different seeds and report the mean and standard deviation.

For the training set, we down-sample 1.5% of protein chains used in OpenFold (Ahdritz et al., 2024), leading to 7,872 chains, with at most 1 protein chain from each cluster. The aggressive down-sampling is supported by the fact that training a protein folding model with as few as 1,000 protein chains achieved a decent performance (Ahdritz et al., 2024). The down-sampled protein chains have lower than 40% sequence identity to each other. We use 95% and 5% as data splitting for training and validation sets. For held-out test sets, we use `CASP15-multimers` (52 protein complexes), `CASP14` (37 protein structures), and `Benchmark2` (17 heterodimers structures) (Ghani et al., 2021). We compare our 740M `LC-PLM` (with `BiMamba` or `BiMamba-S`)

---

[3]We disable attention maps in our experiments since (i) there is no attention map in `BiMamba-S` and (ii) ESMFold (Lin et al., 2023) also demonstrate that attention maps provide no performance gain during training.

[4]ProtMamba is hard to extrapolate on sequence > 2048 since they train with fixed-length positional encodings.

[5]The public ESM-2 model is provided for reference only. We highlight the best results for models trained with the same number of tokens and similar sizes. The tables below follow the same approach.

against 650M ESM-2, all pretrained on 100B tokens from `UniRef50`. `LC-PLM` outperforms ESM-2 across all test sets by a large margin (20.8% on `CASP15-multimers`, 17.6% on `CASP14`, and 29.5% on `Benchmark2`). `LC-PLM` also achieves comparable performance to 650M public ESM-2 model trained on 10× more tokens (1T), with 1.6% improvement on `CASP15-multimers`. These results demonstrate the powerful long-context capability of `BiMamba-S` on modeling longer proteins and protein complexes. This also suggests that, even for average-length protein sequences, long-range dependencies would be useful information and an important feature for protein structure prediction.

5.5 (RQ5) `LC-PLM-G` Encodes Graph Relational Information

To evaluate if `LC-PLM-G` encodes graph relational information, we first conduct the graph-contextual protein language modeling on the PPI graph provided by `ogbn-proteins` dataset Hu et al. (2020), which contains proteins from 8 species, to get a well-trained `LC-PLM-G`. After training, we sample the same number of proteins from each species and obtain their representations using both `LC-PLM` and `LC-PLM-G`. Since we sampled a subset of proteins (nodes) from the dataset, we can use them to construct a subgraph as well. We then use the Louvain algorithm (De Meo et al., 2011) to detect 8 communities (corresponding to 8 species) in this subgraph. Next, we use t-SNE (Van der Maaten & Hinton, 2008) to reduce the dimen-

(a) `LC-PLM`　　　　(b) `LC-PLM-G`

Figure 7: Comparison of t-SNE visualizations on protein-level representations obtained from `LC-PLM` and `LC-PLM-G` with the corresponding community labels detected by the Louvain algorithm on the PPI graph. Embeddings from `LC-PLM-G` recapitulate the topological information.

sionality of both sets of protein embeddings obtained from `LC-PLM` and `LC-PLM-G` and label each data point using its community membership. As shown in Figure 7, the embeddings from `LC-PLM-G` captures the graph topology much better than `LC-PLM`, which aligns with the community detection results. This suggests that our proposed graph context-aware second-stage training captures the topological information in PPI graphs as expected.
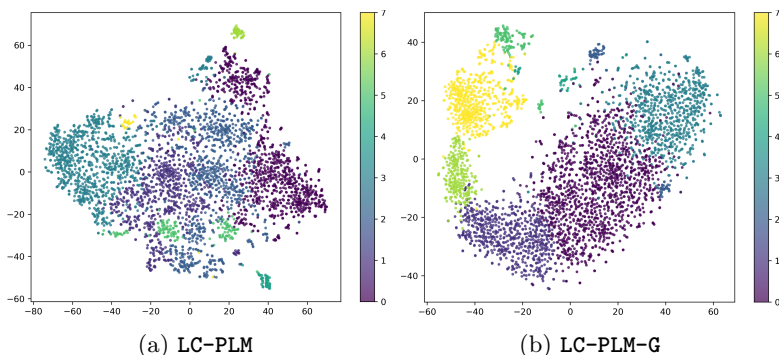
5.6 (RQ6) Interaction Information Helps Downstream Tasks

TAPE　Here we ask whether the graph relational information is helpful for common downstream tasks. We first use the remote homology detection and secondary structure prediction tasks from `TAPE` (Rao et al., 2019), which represent protein-level and residue-level tasks, respectively. Our results in Table 3 show that `LC-PLM` achieves significantly better performance in both tasks compared to ESM-2 pretrained with the same number of tokens. Remarkably, `LC-PLM` and `LC-PLM-G` even outperformed the public ESM-2 pretrained with 1T tokens, underscoring the sample efficiency of `BiMamba-S`-based model architecture can translate to downstream tasks in a supervised fine-tuning setting. The marginal improvement of `LC-PLM-G` over `LC-PLM` in remote homology tasks also suggests the information from the PPI graph helps determine protein's remote homologs, while not helpful in predicting their secondary structures at the AA level.

ProteinGym　Next, we evaluate the predicted fitness landscape on zero-shot mutation effect prediction. It has been shown that pretrained pLMs can capture the fitness landscape of proteins without any further training (Meier et al., 2021). We use 217 deep mutational scan (DMS) datasets collected in `ProteinGym` (Notin et al., 2024), which collectively measure the effects of 2.5 million substitution mutations to parent protein sequences. In Table 4, we demonstrate `LC-PLM` achieved significantly better alignment with protein fitness compared to ESM-2 pretrained with the same number of tokens. Interestingly, we note that the graph-contextual training hurts the fitness landscapes of ESM-2 models, while `LC-PLM-G` retained their

Model (#Tokens trained)	PPI graph	Contact Map	Remote Homology	Secondary Structure	Stability
ESM-2-650M (100B)	None	44.05	26.57 ± 0.49	79.86 ± 0.09	0.763 ± 0.01
ESM-2-G-650M (100B)	ogbn-proteins	32.35	25.60 ± 0.77	79.76 ± 0.24	0.750 ± 0.02
ESM-2-G-650M (100B)	ogbl-ppa	26.66	27.18 ± 0.63	79.91 ± 0.24	0.753 ± 0.01
LC-PLM-740M (100B)	None	47.10	35.14 ± 1.69	85.07 ± 0.03	0.794 ± 0.01
LC-PLM-G-740M (100B)	ogbn-proteins	47.15	**35.74 ± 0.93**	85.02 ± 0.11	0.801 ± 0.01
LC-PLM-G-740M (100B)	ogbl-ppa	47.23	35.60 ± 1.45	85.01 ± 0.03	0.801 ± 0.01
ProtMamba-public	None	10.96	17.82 ± 1.85	68.43 ± 0.06	0.726 ± 0.01
CARP-640M-public	None	25.83	28.0 ± 0.8	83.0 ± 0.1	0.720 ± 0.01
ESM-2-650M-public (1T)	None	**66.85**	33.43 ± 0.35	84.30 ± 0.15	0.804 ± 0.01
LC-PLM-740M (1T)	None	61.93	33.24 ± 0.21	**88.19 ± 0.03**	**0.840 ± 0.02**

Table 3: Evaluation on TAPE tasks in zero-shot (contact map) and supervised fine-tuning (remote homology and secondary structure) settings. We report the *Precision@2/L* for Contact Map prediction, *top-1 accuracy* for the Remote Homology fold-level test set, *accuracy* for the 3-class secondary structure prediction on the CB513 test set, and *spearman's rho* for stability prediction, respectively. Values for CARP are taken from Yang et al. (2024). We perform 3 runs using different seeds to report the mean and standard deviation.

zero-shot capabilities for protein fitness prediction. We hypothesize that the long graph context degrades the representation space of ESM-2, not for LC-PLM-G. This highlights BiMamba-S as a superior architectural design choice, demonstrating robustness in maintaining performance across various tasks while excelling in those that benefit from interaction information learned through graph-contextualized training, possibly due to its preferable context-length extrapolation property.

Model (#Tokens trained)	PPI graph	Spearman	NDCG
ESM-2-650M (100B)	None	0.295 ± 0.013	0.695 ± 0.008
ESM-2-G-650M (100B)	ogbn-proteins	0.109 ± 0.013	0.642 ± 0.008
ESM-2-G-650M (100B)	ogbl-ppa	0.131 ± 0.014	0.644 ± 0.007
LC-PLM-740M (100B)	None	0.378 ± 0.008	**0.735 ± 0.005**
LC-PLM-G-740M (100B)	ogbn-proteins	**0.380 ± 0.008**	0.734 ± 0.006
LC-PLM-G-740M (100B)	ogbl-ppa	**0.380 ± 0.008**	0.734 ± 0.006

Table 4: Evaluation on ProteinGym DMS substitutions benchmark. We report *Spearman's correlation coefficient* and *normalized discounted cumulative gain (NDCG)* between the log odds ratio and the experimentally measured protein fitness scores for each DMS assay.

5.7 (RQ7) Protein Function Prediction and Link Prediction on PPI Graph

We evaluate LC-PLM-G on two tasks: protein function prediction (ogbn-proteins) and PPI link prediction (ogbl-ppa). On ogbn-proteins, LC-PLM-G achieves an *accuracy* of 0.8925 ± 0.001, outperforming the state-of-the-art by 2.6%. For ogbl-ppa, we leverage the learned embeddings from both LC-PLM and LC-PLM-G to initialize the node attributes for GCN and GraphSAGE, evaluating these model variants. The results confirm that the embeddings improve performance. We conduct similar experiments on ogbn-proteins, further validating the effectiveness of capturing graph-contextual information. Additional details are provided in Appendix H.

6 Conclusion, Discussion, and Future Work

In this work, we explored `LC-PLM` and `LC-PLM-G` based on `BiMamba-S`. We demonstrate `LC-PLM`'s favorable neural scaling laws and length extrapolation property than Transformer-based ESM-2. We found that the length extrapolation property can facilitate the 3-D structure prediction of longer proteins and protein complexes. Specifically, `LC-PLM` outperformed ESM-2 by up to 30% and 16% on various downstream tasks when trained with 100B and 1T tokens, respectively. We also found that after training within graph context using random walk sampling, `LC-PLM-G` can capture relational structure encoded in protein-protein interactions and improve remote homology prediction by more than 35% compared to ESM-2.

`LC-PLM` not only demonstrates superior performance on longer protein sequences but also outperforms ESM-2 on shorter protein sequences, highlighting a significant performance gap between SSMs and Transformers in protein language modeling. We hypothesize that this advantage may be attributed to the relatively small vocabulary size of protein sequences (~ 20 tokens), which allows SSMs to more effectively learn compressed state representations compared to natural languages, where the vocabulary size typically exceeds 50k tokens.

It is also possible that ESM-2 could incorporate more advanced architectural designs within its Transformer-based framework to narrow the performance gap, given the rapid advancements in text modeling and Transformer architectures. There are also emerging techniques that may further assist ESM-2 in bridging the gap in long-context modeling capability compared to `LC-PLM`.

In future work, we aim to (i) explore hybrid architectures that integrate multi-head attention with SSMs, (ii) investigate more advanced self-supervised training strategies to enhance the incorporation of graph-contextual information during the later stages of pre-training, e.g., contrastive learning using *(positive, negative)* pairs of random walk paths to reinforce locality relationships, and (iii) develop more principled approaches for negative sampling to better contrast with *positive* random walk paths. Some other directions include (i) approximate permutation-invariant graph context learning for pLMs, e.g. using permutation group (Huang et al., 2022), (ii) explore other graph context extraction methods instead of random walk, e.g. graph skeleton tree (Huang et al., 2023).

We also think it deserves to expand the application scope of `LC-PLM` across several key areas: (i) understanding viral protein sequences, which are characterized by extended sequence lengths; (ii) enhancement of protein co-regulation and functional prediction capabilities (Hwang et al., 2024); and (iii) advanced protein design tasks requiring expanded contextual understanding, such as protein inpainting. We anticipate that `LC-PLM`'s capabilities will enable novel applications beyond these identified domains, presenting significant opportunities for further exploration in the field of protein modeling and design.

References

Gustaf Ahdritz, Nazim Bouatta, Christina Floristean, Sachin Kadyan, Qinghui Xia, William Gerecke, Timothy J O'Donnell, Daniel Berenberg, Ian Fisk, Niccolò Zanichelli, et al. Openfold: Retraining alphafold2 yields new insights into its learning mechanisms and capacity for generalization. *Nature Methods*, pp. 1–11, 2024.

Ethan C. Alley, Grigory Khimulya, Surojit Biswas, Mohammed AlQuraishi, and George M. Church. Unified rational protein engineering with sequence-based deep representation learning. *Nature Methods*, 2019a.

Ethan C Alley, Grigory Khimulya, Surojit Biswas, Mohammed AlQuraishi, and George M Church. Unified rational protein engineering with sequence-based deep representation learning. *Nature methods*, 16(12): 1315–1322, 2019b.

Mohammed AlQuraishi. Proteinnet: a standardized data set for machine learning of protein structure. *BMC bioinformatics*, 20:1–10, 2019.

Simran Arora, Sabri Eyuboglu, Michael Zhang, Aman Timalsina, Silas Alberti, Dylan Zinsley, James Zou, Atri Rudra, and Christopher Ré. Simple linear attention language models balance the recall-throughput tradeoff. *arXiv preprint arXiv:2402.18668*, 2024.

Ehsaneddin Asgari, Nina Poerner, Alice C. McHardy, and Mohammad R. K. Mofrad. Deepprime2sec: Deep learning for protein secondary structure prediction from the primary sequences. *bioRxiv*, 2019.

Jürgen Bajorath. Integration of virtual and high-throughput screening. *Nature Reviews Drug Discovery*, 1 (11):882–894, 2002.

Ali Behrouz and Farnoosh Hashemi. Graph mamba: Towards learning on graphs with state space models, 2024. URL https://arxiv.org/abs/2402.08678.

Y. Bengio, P. Simard, and P. Frasconi. Learning long-term dependencies with gradient descent is difficult. *IEEE Transactions on Neural Networks*, 5(2):157–166, 1994. doi: 10.1109/72.279181.

Tristan Bepler and Bonnie Berger. Learning the protein language: Evolution, structure, and function. *Cell systems*, 2021.

Aleksandar Botev, Soham De, Samuel L Smith, Anushan Fernando, George-Cristian Muraru, Ruba Haroun, Leonard Berrada, Razvan Pascanu, Pier Giuseppe Sessa, Robert Dadashi, et al. Recurrentgemma: Moving past transformers for efficient open language models. *arXiv preprint arXiv:2404.07839*, 2024.

Emmanuel Boutet, Damien Lieberherr, Michael Tognolli, Michel Schneider, Parit Bansal, Alan J Bridge, Sylvain Poux, Lydie Bougueleret, and Ioannis Xenarios. Uniprotkb/swiss-prot, the manually annotated section of the uniprot knowledgebase: how to use the entry view. *Plant bioinformatics: methods and protocols*, pp. 23–54, 2016.

Ratul Chowdhury, Nazim Bouatta, Surojit Biswas, Charlotte Rochereau, George M. Church, Peter K. Sorger, and Mohammed AlQuraishi. Single-sequence protein structure prediction using language models from deep learning. *Nature Biotechnology*, 2022.

Tri Dao and Albert Gu. Transformers are ssms: Generalized models and efficient algorithms through structured state space duality. *arXiv preprint arXiv:2405.21060*, 2024.

Soham De, Samuel L. Smith, Anushan Fernando, Aleksandar Botev, George Cristian-Muraru, Albert Gu, Ruba Haroun, Leonard Berrada, Yutian Chen, Srivatsan Srinivasan, Guillaume Desjardins, Arnaud Doucet, David Budden, Yee Whye Teh, Razvan Pascanu, Nando De Freitas, and Caglar Gulcehre. Griffin: Mixing gated linear recurrences with local attention for efficient language models, 2024. URL https://arxiv.org/abs/2402.19427.

Pasquale De Meo, Emilio Ferrara, Giacomo Fiumara, and Alessandro Provetti. Generalized louvain method for community detection in large networks. In *2011 11th international conference on intelligent systems design and applications*, pp. 88–93. IEEE, 2011.

Nicki Skafte Detlefsen, Søren Hauberg, and Wouter Boomsma. Learning meaningful representations of protein sequences. *Nature communications*, 13(1):1914, 2022.

Jacob Devlin. Bert: Pre-training of deep bidirectional transformers for language understanding. *arXiv preprint arXiv:1810.04805*, 2018.

Ahmed Elnaggar, Michael Heinzinger, Christian Dallago, Ghalia Rehawi, Wang Yu, Llion Jones, Tom Gibbs, Tamas Feher, Christoph Angerer, Martin Steinegger, Debsindhu Bhowmik, and Burkhard Rost. Prottrans: Towards cracking the language of lifes code through self-supervised deep learning and high performance computing. *IEEE Transactions on Pattern Analysis and Machine Intelligence*, 2021.

Mehmet Hamza Erol, Arda Senocak, Jiu Feng, and Joon Son Chung. Audio mamba: Bidirectional state space model for audio representation learning. *arXiv preprint arXiv:2406.03344*, 2024.

Kawin Ethayarajh. How contextual are contextualized word representations? comparing the geometry of bert, elmo, and gpt-2 embeddings. *arXiv preprint arXiv:1909.00512*, 2019.

Noelia Ferruz, Steffen Schmidt, and Birte Höcker. Protgpt2 is a deep unsupervised language model for protein design. *Nature communications*, 13(1):4348, 2022.

Daniel Y Fu, Tri Dao, Khaled K Saab, Armin W Thomas, Atri Rudra, and Christopher Ré. Hungry hungry hippos: Towards language modeling with state space models. *arXiv preprint arXiv:2212.14052*, 2022.

Jun Gao, Di He, Xu Tan, Tao Qin, Liwei Wang, and Tie-Yan Liu. Representation degeneration problem in training natural language generation models. *arXiv preprint arXiv:1907.12009*, 2019.

Usman Ghani, Israel Desta, Akhil Jindal, Omeir Khan, George Jones, Nasser Hashemi, Sergey Kotelnikov, Dzmitry Padhorny, Sandor Vajda, and Dima Kozakov. Improved docking of protein models by a combination of alphafold2 and cluspro. *BioRxiv*, pp. 2021–09, 2021.

Aditya Grover and Jure Leskovec. node2vec: Scalable feature learning for networks. In *Proceedings of the 22nd ACM SIGKDD international conference on Knowledge discovery and data mining*, pp. 855–864, 2016.

Albert Gu and Tri Dao. Mamba: Linear-time sequence modeling with selective state spaces, 2024. URL https://arxiv.org/abs/2312.00752.

Albert Gu, Tri Dao, Stefano Ermon, Atri Rudra, and Christopher Ré. Hippo: Recurrent memory with optimal polynomial projections. *Advances in neural information processing systems*, 33:1474–1487, 2020.

Albert Gu, Karan Goel, and Christopher Ré. Efficiently modeling long sequences with structured state spaces. *arXiv preprint arXiv:2111.00396*, 2021.

Will Hamilton, Zhitao Ying, and Jure Leskovec. Inductive representation learning on large graphs. *Advances in neural information processing systems*, 30, 2017.

Liang He, Shizhuo Zhang, Lijun Wu, Huanhuan Xia, Fusong Ju, He Zhang, Siyuan Liu, Yingce Xia, Jianwei Zhu, Pan Deng, Bin Shao, Tao Qin, and Tie-Yan Liu. Pre-training co-evolutionary protein representation via a pairwise masked language model. 2022.

Rhys Heffernan, Kuldip K. Paliwal, James Lyons, Jaswinder Singh, Yuedong Yang, and Yaoqi Zhou. Single-sequence-based prediction of protein secondary structures and solvent accessibility by deep whole-sequence learning. *Journal of Computational Chemistry*, 2018.

Michael Heinzinger, Ahmed Elnaggar, Yu Wang, Christian Dallago, Dmitrii Nechaev, Florian Matthes, and Burkhard Rost. Modeling the language of life – deep learning protein sequences. *bioRxiv*, 2019.

Sepp Hochreiter. Untersuchungen zu dynamischen neuronalen netzen. *Diploma, Technische Universität München*, 91(1), 1991.

Sepp Hochreiter and Jürgen Schmidhuber. Long short-term memory. *Neural computation*, 9:1735–80, 12 1997. doi: 10.1162/neco.1997.9.8.1735.

Bozhen Hu, Jun Xia, Jiangbin Zheng, Cheng Tan, Yufei Huang, Yongjie Xu, and Stan Z Li. Protein language models and structure prediction: Connection and progression. *arXiv preprint arXiv:2211.16742*, 2022.

Weihua Hu, Matthias Fey, Marinka Zitnik, Yuxiao Dong, Hongyu Ren, Bowen Liu, Michele Catasta, and Jure Leskovec. Open graph benchmark: Datasets for machine learning on graphs. *Advances in neural information processing systems*, 33:22118–22133, 2020.

Zhongyu Huang, Yingheng Wang, Chaozhuo Li, and Huiguang He. Going deeper into permutation-sensitive graph neural networks. In *International Conference on Machine Learning*, pp. 9377–9409. PMLR, 2022.

Zhongyu Huang, Yingheng Wang, Chaozhuo Li, and Huiguang He. Growing like a tree: Finding trunks from graph skeleton trees. *IEEE Transactions on Pattern Analysis and Machine Intelligence*, 2023.

Yunha Hwang, Andre L Cornman, Elizabeth H Kellogg, Sergey Ovchinnikov, and Peter R Girguis. Genomic language model predicts protein co-regulation and function. *Nature communications*, 15(1):2880, 2024.

John Jumper, Richard Evans, Alexander Pritzel, Tim Green, Michael Figurnov, Olaf Ronneberger, Kathryn Tunyasuvunakool, Russ Bates, Augustin Žídek, Anna Potapenko, et al. Highly accurate protein structure prediction with alphafold. *nature*, 596(7873):583–589, 2021.

Angelos Katharopoulos, Apoorv Vyas, Nikolaos Pappas, and François Fleuret. Transformers are rnns: Fast autoregressive transformers with linear attention. In *International conference on machine learning*, pp. 5156–5165. PMLR, 2020.

Thomas N Kipf and Max Welling. Semi-supervised classification with graph convolutional networks. *ICLR*, 2017.

Michael Schantz Klausen, Martin Closter Jespersen, Henrik Nielsen, Kamilla Kjærgaard Jensen, Vanessa Isabell Jurtz, Casper Kaae Sønderby, Morten Otto Alexander Sommer, Ole Winther, Morten Nielsen, Bent O. Petersen, and Paolo Marcatili. Netsurfp-2.0: improved prediction of protein structural features by integrated deep learning. *Proteins*, 2018.

István A Kovács, Katja Luck, Kerstin Spirohn, Yang Wang, Carl Pollis, Sadie Schlabach, Wenting Bian, Dae-Kyum Kim, Nishka Kishore, Tong Hao, et al. Network-based prediction of protein interactions. *Nature communications*, 10(1):1240, 2019.

Ben Krause, Liang Lu, Iain Murray, and Steve Renals. Multiplicative lstm for sequence modelling. *Learning*, 2016.

Andriy Kryshtafovych, Torsten Schwede, Maya Topf, Krzysztof Fidelis, and John Moult. Critical assessment of methods of protein structure prediction (casp)—round xiv. *Proteins: Structure, Function, and Bioinformatics*, 89(12):1607–1617, 2021.

Andriy Kryshtafovych, Torsten Schwede, Maya Topf, Krzysztof Fidelis, and John Moult. Critical assessment of methods of protein structure prediction (casp)—round xv. *Proteins: Structure, Function, and Bioinformatics*, 91(12):1539–1549, 2023.

Guohao Li, Matthias Muller, Ali Thabet, and Bernard Ghanem. Deepgcns: Can gcns go as deep as cnns? In *Proceedings of the IEEE/CVF international conference on computer vision*, pp. 9267–9276, 2019.

Guohao Li, Chenxin Xiong, Ali Thabet, and Bernard Ghanem. Deepergcn: All you need to train deeper gcns. *arXiv preprint arXiv:2006.07739*, 2020.

Houyi Li, Zhihong Chen, Zhao Li, Qinkai Zheng, Peng Zhang, and Shuigeng Zhou. Gipa: A general information propagation algorithm for graph learning. In *International Conference on Database Systems for Advanced Applications*, pp. 465–476. Springer, 2023.

Aobo Liang, Xingguo Jiang, Yan Sun, and Chang Lu. Bi-mamba4ts: Bidirectional mamba for time series forecasting. *arXiv preprint arXiv:2404.15772*, 2024.

Opher Lieber, Barak Lenz, Hofit Bata, Gal Cohen, Jhonathan Osin, Itay Dalmedigos, Erez Safahi, Shaked Meirom, Yonatan Belinkov, Shai Shalev-Shwartz, et al. Jamba: A hybrid transformer-mamba language model. *arXiv preprint arXiv:2403.19887*, 2024.

Zeming Lin, Halil Akin, Roshan Rao, Brian Hie, Zhongkai Zhu, Wenting Lu, Nikita Smetanin, Robert Verkuil, Ori Kabeli, Yaniv Shmueli, et al. Evolutionary-scale prediction of atomic-level protein structure with a language model. *Science*, 379(6637):1123–1130, 2023.

Amy X. Lu, Haoran Zhang, Marzyeh Ghassemi, and Alan M. Moses. Self-supervised contrastive learning of protein representations by mutual information maximization. *bioRxiv*, 2020.

Ricardo Macarron, Martyn N Banks, Dejan Bojanic, David J Burns, Dragan A Cirovic, Tina Garyantes, Darren VS Green, Robert P Hertzberg, William P Janzen, Jeff W Paslay, et al. Impact of high-throughput screening in biomedical research. *Nature reviews Drug discovery*, 10(3):188–195, 2011.

Ali Madani, Bryan McCann, Nikhil Naik, Nitish Shirish Keskar, Namrata Anand, Raphael R. Eguchi, Po-Ssu Huang, and Richard Socher. Progen: Language modeling for protein generation, 2020.

Matthew BA McDermott, Brendan Yap, Peter Szolovits, and Marinka Zitnik. Structure-inducing pre-training. *Nature Machine Intelligence*, 5(6):612–621, 2023.

Joshua Meier, Roshan Rao, Robert Verkuil, Jason Liu, Tom Sercu, and Alex Rives. Language models enable zero-shot prediction of the effects of mutations on protein function. *Advances in neural information processing systems*, 34:29287–29303, 2021.

James T. Morton, Strauss Cem, Blackwell R, Daniel Berenberg, Gligorijevic, and Richard Bonneau. Protein structural alignments from sequence. *bioRxiv*, 2020.

Eric Nguyen, Michael Poli, Matthew G Durrant, Armin W Thomas, Brian Kang, Jeremy Sullivan, Madelena Y Ng, Ashley Lewis, Aman Patel, Aaron Lou, et al. Sequence modeling and design from molecular to genome scale with evo. *BioRxiv*, pp. 2024–02, 2024a.

Eric Nguyen, Michael Poli, Marjan Faizi, Armin Thomas, Michael Wornow, Callum Birch-Sykes, Stefano Massaroli, Aman Patel, Clayton Rabideau, Yoshua Bengio, et al. Hyenadna: Long-range genomic sequence modeling at single nucleotide resolution. *Advances in neural information processing systems*, 36, 2024b.

Erik Nijkamp, Jeffrey Ruffolo, Eli N Weinstein, Nikhil Naik, Ali Madani, and Salesforce Research. Progen2: Exploring the boundaries of protein language models. 2022.

Pascal Notin, Lood Van Niekerk, Aaron W Kollasch, Daniel Ritter, Yarin Gal, and Debora S Marks. Trancepteve: Combining family-specific and family-agnostic models of protein sequences for improved fitness prediction. *bioRxiv*, pp. 2022–12, 2022.

Pascal Notin, Aaron Kollasch, Daniel Ritter, Lood Van Niekerk, Steffanie Paul, Han Spinner, Nathan Rollins, Ada Shaw, Rose Orenbuch, Ruben Weitzman, et al. Proteingym: Large-scale benchmarks for protein fitness prediction and design. *Advances in Neural Information Processing Systems*, 36, 2024.

Chigozie Nwankpa, Winifred Ijomah, Anthony Gachagan, and Stephen Marshall. Activation functions: Comparison of trends in practice and research for deep learning. *arXiv preprint arXiv:1811.03378*, 2018.

Dan Ofer, Nadav Brandes, and Michal Linial. The language of proteins: Nlp, machine learning & protein sequences. *Computational and Structural Biotechnology Journal*, 19:1750–1758, 2021a. ISSN 2001-0370. doi: https://doi.org/10.1016/j.csbj.2021.03.022. URL https://www.sciencedirect.com/science/article/pii/S2001037021000945.

Dan Ofer, Nadav Brandes, Michal Linial, Nadav Rappoport, and Yam Peleg. Proteinbert: A universal deep-learning model of protein sequence and function. *F1000Research*, 2021b.

Bo Peng, Eric Alcaide, Quentin Anthony, Alon Albalak, Samuel Arcadinho, Stella Biderman, Huanqi Cao, Xin Cheng, Michael Chung, Matteo Grella, et al. Rwkv: Reinventing rnns for the transformer era. *arXiv preprint arXiv:2305.13048*, 2023.

Zhangzhi Peng, Benjamin Schussheim, and Pranam Chatterjee. Ptm-mamba: A ptm-aware protein language model with bidirectional gated mamba blocks. *bioRxiv*, 2024.

Bryan Perozzi, Rami Al-Rfou, and Steven Skiena. Deepwalk: Online learning of social representations. In *Proceedings of the 20th ACM SIGKDD international conference on Knowledge discovery and data mining*, pp. 701–710, 2014.

Michael Poli, Stefano Massaroli, Eric Nguyen, Daniel Y Fu, Tri Dao, Stephen Baccus, Yoshua Bengio, Stefano Ermon, and Christopher Ré. Hyena hierarchy: Towards larger convolutional language models. In *International Conference on Machine Learning*, pp. 28043–28078. PMLR, 2023.

Roshan Rao, Nicholas Bhattacharya, Neil Thomas, Yan Duan, Peter Chen, John Canny, Pieter Abbeel, and Yun Song. Evaluating protein transfer learning with tape. *Advances in neural information processing systems*, 32, 2019.

Roshan Rao, Joshua Meier, Tom Sercu, Sergey Ovchinnikov, and Alexander Rives. Transformer protein language models are unsupervised structure learners. *Biorxiv*, pp. 2020–12, 2020.

Roshan Rao, Jason Liu, Robert Verkuil, Joshua Meier, John Canny, Pieter Abbeel, Tom Sercu, and Alexander Rives. Msa transformer. *bioRxiv*, 2021.

Alexander Rives, Siddharth Goyal, Joshua Meier, Demi Guo, Myle Ott, C. Lawrence Zitnick, Jerry Ma, and Rob Fergus. Biological structure and function emerge from scaling unsupervised learning to 250 million protein sequences. *Proceedings of the National Academy of Sciences of the United States of America*, 2019.

Alexander Rives, Joshua Meier, Tom Sercu, Siddharth Goyal, Zeming Lin, Jason Liu, Demi Guo, Myle Ott, C Lawrence Zitnick, Jerry Ma, et al. Biological structure and function emerge from scaling unsupervised learning to 250 million protein sequences. *Proceedings of the National Academy of Sciences*, 118(15): e2016239118, 2021.

Yair Schiff, Chia-Hsiang Kao, Aaron Gokaslan, Tri Dao, Albert Gu, and Volodymyr Kuleshov. Caduceus: Bi-directional equivariant long-range dna sequence modeling. *arXiv preprint arXiv:2403.03234*, 2024.

Damiano Sgarbossa, Cyril Malbranke, and Anne-Florence Bitbol. Protmamba: a homology-aware but alignment-free protein state space model. *bioRxiv*, pp. 2024–05, 2024.

Yunsheng Shi, Zhengjie Huang, Shikun Feng, Hui Zhong, Wenjin Wang, and Yu Sun. Masked label prediction: Unified message passing model for semi-supervised classification. *arXiv preprint arXiv:2009.03509*, 2020.

Jaspreet Singh, Thomas Litfin, Kuldip K. Paliwal, Jaswinder Singh, Anil Kumar Hanumanthappa, and Yaoqi Zhou. Spot-1d-single: Improving the single-sequence-based prediction of protein secondary structure, backbone angles, solvent accessibility and half-sphere exposures using a large training set and ensembled deep learning. *Bioinformatics*, 2021a.

Jaspreet Singh, Thomas Litfin, Jaswinder Singh, Kuldip K. Paliwal, and Yaoqi Zhou. Spot-contact-single: Improving single-sequence-based prediction of protein contact map using a transformer language model. *bioRxiv*, 2021b.

Jaspreet Singh, Kuldip K. Paliwal, Jaswinder Singh, and Yaoqi Zhou. Spot-1d-lm: Reaching alignment-profile-based accuracy in predicting protein secondary and tertiary structural properties without alignment. *bioRxiv*, 2021c.

Xiang Song, Runjie Ma, Jiahang Li, Muhan Zhang, and David Paul Wipf. Network in graph neural network. *arXiv preprint arXiv:2111.11638*, 2021.

Rita T Sousa, Sara Silva, and Catia Pesquita. Explaining protein–protein interactions with knowledge graph-based semantic similarity. *Computers in Biology and Medicine*, 170:108076, 2024.

Martin Steinegger and Johannes Söding. Mmseqs2 enables sensitive protein sequence searching for the analysis of massive data sets. *Nature biotechnology*, 35(11):1026–1028, 2017.

Nils Strodthoff, Patrick Wagner, Markus Wenzel, and Wojciech Samek. UDSMProt: universal deep sequence models for protein classification. *Bioinformatics*, 36(8):2401–2409, 01 2020. ISSN 1367-4803. doi: 10.1093/bioinformatics/btaa003.

Jianlin Su, Murtadha Ahmed, Yu Lu, Shengfeng Pan, Wen Bo, and Yunfeng Liu. Roformer: Enhanced transformer with rotary position embedding. *Neurocomputing*, 568:127063, 2024.

Jin Su, Chenchen Han, Yuyang Zhou, Junjie Shan, Xibin Zhou, and Fajie Yuan. Saprot: Protein language modeling with structure-aware vocabulary. *bioRxiv*, pp. 2023–10, 2023.

Mingjie Sun, Xinlei Chen, J Zico Kolter, and Zhuang Liu. Massive activations in large language models. *arXiv preprint arXiv:2402.17762*, 2024.

Yutao Sun, Li Dong, Barun Patra, Shuming Ma, Shaohan Huang, Alon Benhaim, Vishrav Chaudhary, Xia Song, and Furu Wei. A length-extrapolatable transformer. *arXiv preprint arXiv:2212.10554*, 2022.

Baris E Suzek, Yuqi Wang, Hongzhan Huang, Peter B McGarvey, Cathy H Wu, and UniProt Consortium. Uniref clusters: a comprehensive and scalable alternative for improving sequence similarity searches. *Bioinformatics*, 31(6):926–932, 2015.

Damian Szklarczyk, Annika L Gable, David Lyon, Alexander Junge, Stefan Wyder, Jaime Huerta-Cepas, Milan Simonovic, Nadezhda T Doncheva, John H Morris, Peer Bork, et al. String v11: protein–protein association networks with increased coverage, supporting functional discovery in genome-wide experimental datasets. *Nucleic acids research*, 47(D1):D607–D613, 2019.

Matus Telgarsky. Benefits of depth in neural networks. In *Conference on learning theory*, pp. 1517–1539. PMLR, 2016.

Timothy Truong Jr and Tristan Bepler. Poet: A generative model of protein families as sequences-of-sequences. *Advances in Neural Information Processing Systems*, 36:77379–77415, 2023.

Timothy Truong Jr and Tristan Bepler. Poet: A generative model of protein families as sequences-of-sequences. *Advances in Neural Information Processing Systems*, 36, 2024.

Laurens Van der Maaten and Geoffrey Hinton. Visualizing data using t-sne. *Journal of machine learning research*, 9(11), 2008.

Ashish Vaswani, Noam Shazeer, Niki Parmar, Jakob Uszkoreit, Llion Jones, Aidan N Gomez, Łukasz Kaiser, and Illia Polosukhin. Attention is all you need. *Advances in neural information processing systems*, 30, 2017.

Petar Veličković, Guillem Cucurull, Arantxa Casanova, Adriana Romero, Pietro Lio, and Yoshua Bengio. Graph attention networks. *arXiv preprint arXiv:1710.10903*, 2017.

Roger Waleffe, Wonmin Byeon, Duncan Riach, Brandon Norick, Vijay Korthikanti, Tri Dao, Albert Gu, Ali Hatamizadeh, Sudhakar Singh, Deepak Narayanan, et al. An empirical study of mamba-based language models. *arXiv preprint arXiv:2406.07887*, 2024.

Chloe Wang, Oleksii Tsepa, Jun Ma, and Bo Wang. Graph-mamba: Towards long-range graph sequence modeling with selective state spaces, 2024. URL https://arxiv.org/abs/2402.00789.

Yingheng Wang, Xin Chen, Yaosen Min, and Ji Wu. Molcloze: a unified cloze-style self-supervised molecular structure learning model for chemical property prediction. In *2021 IEEE International Conference on Bioinformatics and Biomedicine (BIBM)*, pp. 2896–2903. IEEE, 2021a.

Yingheng Wang, Yaosen Min, Xin Chen, and Ji Wu. Multi-view graph contrastive representation learning for drug-drug interaction prediction. In *Proceedings of the Web Conference 2021*, pp. 2921–2933, 2021b.

Yingheng Wang, Yaosen Min, Erzhuo Shao, and Ji Wu. Molecular graph contrastive learning with parameterized explainable augmentations. In *2021 IEEE International Conference on Bioinformatics and Biomedicine (BIBM)*, pp. 1558–1563. IEEE, 2021c.

Zichen Wang, Vassilis N Ioannidis, Huzefa Rangwala, Tatsuya Arai, Ryan Brand, Mufei Li, and Yohei Nakayama. Graph neural networks in life sciences: opportunities and solutions. In *Proceedings of the 28th ACM SIGKDD Conference on Knowledge Discovery and Data Mining*, pp. 4834–4835, 2022.

Zifeng Wang, Zichen Wang, Balasubramaniam Srinivasan, Vassilis N Ioannidis, Huzefa Rangwala, and Rishita Anubhai. Biobridge: Bridging biomedical foundation models via knowledge graph. *arXiv preprint arXiv:2310.03320*, 2023.

Minghao Xu, Zuobai Zhang, Jiarui Lu, Zhaocheng Zhu, Yangtian Zhang, Chang Ma, Runcheng Liu, and Jian Tang. Peer: A comprehensive and multi-task benchmark for protein sequence understanding. 2022.

Kevin K Yang, Nicolo Fusi, and Alex X Lu. Convolutions are competitive with transformers for protein sequence pretraining. *Cell Systems*, 15(3):286–294, 2024.

Michihiro Yasunaga, Jure Leskovec, and Percy Liang. Linkbert: Pretraining language models with document links. *arXiv preprint arXiv:2203.15827*, 2022.

David Younger, Stephanie Berger, David Baker, and Eric Klavins. High-throughput characterization of protein–protein interactions by reprogramming yeast mating. *Proceedings of the National Academy of Sciences*, 114(46):12166–12171, 2017.

Luca Zancato, Arjun Seshadri, Yonatan Dukler, Aditya Golatkar, Yantao Shen, Benjamin Bowman, Matthew Trager, Alessandro Achille, and Stefano Soatto. B'mojo: Hybrid state space realizations of foundation models with eidetic and fading memory. *arXiv preprint arXiv:2407.06324*, 2024.

Shuangfei Zhai, Walter Talbott, Nitish Srivastava, Chen Huang, Hanlin Goh, Ruixiang Zhang, and Josh Susskind. An attention free transformer. *arXiv preprint arXiv:2105.14103*, 2021.

Muhan Zhang and Yixin Chen. Link prediction based on graph neural networks. *Advances in neural information processing systems*, 31, 2018.

Muhan Zhang, Zhicheng Cui, Marion Neumann, and Yixin Chen. An end-to-end deep learning architecture for graph classification. In *Proceedings of the AAAI conference on artificial intelligence*, volume 32, 2018.

Muhan Zhang, Pan Li, Yinglong Xia, Kai Wang, and Long Jin. Labeling trick: A theory of using graph neural networks for multi-node representation learning. *Advances in Neural Information Processing Systems*, 34: 9061–9073, 2021.

Ningyu Zhang, Zhen Bi, Xiaozhuan Liang, Siyuan Cheng, Haosen Hong, Shumin Deng, Jiazhang Lian, Qiang Zhang, and Huajun Chen. Ontoprotein: Protein pretraining with gene ontology embedding. *arXiv preprint arXiv:2201.11147*, 2022.

Xiangyu Zhang, Qiquan Zhang, Hexin Liu, Tianyi Xiao, Xinyuan Qian, Beena Ahmed, Eliathamby Ambikairajah, Haizhou Li, and Julien Epps. Mamba in speech: Towards an alternative to self-attention. *arXiv preprint arXiv:2405.12609*, 2024a.

Yiming Zhang. Prothyena: A fast and efficient foundation protein language model at single amino acid resolution. *bioRxiv*, pp. 2024–01, 2024.

Zhidian Zhang, Hannah K Wayment-Steele, Garyk Brixi, Haobo Wang, Dorothee Kern, and Sergey Ovchinnikov. Protein language models learn evolutionary statistics of interacting sequence motifs. *Proceedings of the National Academy of Sciences*, 121(45):e2406285121, 2024b.

Liang Zhao, Xiaocheng Feng, Xiachong Feng, Bin Qin, and Ting Liu. Length extrapolation of transformers: A survey from the perspective of position encoding. *arXiv preprint arXiv:2312.17044*, 2023.

Tong Zhao, Wei Jin, Yozen Liu, Yingheng Wang, Gang Liu, Stephan Günnemann, Neil Shah, and Meng Jiang. Graph data augmentation for graph machine learning: A survey. *arXiv preprint arXiv:2202.08871*, 2022.

Lianghui Zhu, Bencheng Liao, Qian Zhang, Xinlong Wang, Wenyu Liu, and Xinggang Wang. Vision mamba: Efficient visual representation learning with bidirectional state space model. *arXiv preprint arXiv:2401.09417*, 2024.

Contents

Appendices

Appendix A   Definitions of Criterions Used in Table 1

Here, we provide clear definitions for all criteria listed in Table 1 and explain the rationale for whether each method possesses the corresponding feature.

- **Universality**: We define this criteria and justify whether a method possesses this feature (1) if it is *learning universal, cross-family representations of protein space* as defined in previous works of protein representation learning (Alley et al., 2019b; Detlefsen et al., 2022); and (2) if it is pretrained on universal protein dataset, e.g. the *Universal* Protein Reference Clusters (UniRef) dataset which contains universal protein sequence resources; (3) if the learned expressive protein/AA embeddings can achieve decent performance across a variety of downstream tasks, which demonstrates the universality of such representations.

- **Fine granularity**: given that the protein sequence is composed of high-resolution AA tokens, we define this criteria according to whether the model can take in AA token as input. Note that Graph-Mamba (Wang et al., 2024) and GMN (Behrouz & Hashemi, 2024) can only handle inputs like PPI graphs where each node corresponds to an individual protein.

- **Long-context capability (Handleability)**: we define this criteria according to whether the model can take in extremely long (e.g. $> 16K$ sequence length) input sequence. Note that Transformers naturally lack this feature and ProtMamba (Sgarbossa et al., 2024) discards this capability by improperly using positional encodings (PEs)[6] which makes it unable to extrapolate to sequences > 2048 on any downstream tasks that need fine-tuning on longer sequences as we discussed in the main text. ProtMamba used learnable PE as an improper design choice that will do harm to the length extrapolation capability of the model since such PE has been demonstrated as an un-extrapolatable PE in many works (Zhao et al., 2023; Sun et al., 2022).

- **Long-context capability (Performance)**: we define this criteria according to whether the model can perform well across a variety of downstream tasks that need long-context dependencies (e.g. structure prediction on protein complex, remote homology prediction).

- **Graph context**: we define this criteria according to whether the model can take into account the protein interaction graph contexts. All models purely based on protein sequence fail.

- **Large-scale model**: we define this criteria according to whether the model has been scaled up to a fairly large size (e.g. the number of trainable model parameters closer to 1B).

Appendix B   More Discussion on General pLMs

As noted earlier, protein sequences, represented as strings of amino acid letters, are well-suited to LMs that can capture complex dependencies among amino acids (Ofer et al., 2021a). pLMs (Hu et al., 2022) have emerged as promising tools for learning protein sequences. This section introduces LSTM-based pLMs, followed by Transformer-based pLMs, detailing their implementation strategies and applications, particularly for protein structure prediction.

Klausen et al. (2018) developed a combination of convolutional and LSTM neural networks to predict various protein structural features, such as solvent accessibility, secondary structure, structural disorder, and torsion angles (φ, ψ) for each residue. Models like SPIDER3-Single (Heffernan et al., 2018) focus on single sequences rather than relying on multiple sequence alignments (MSAs). Similarly, models such as DeepPrime2Sec (Asgari et al., 2019) and SPOT-1D-Single (Singh et al., 2021a) share comparable training objectives and architectures. Furthermore, models like DeepBLAST (Morton et al., 2020), SPOT-1D-LM (Singh et al., 2021c), and SPOT-Contact-Single (Singh et al., 2021b) utilize embeddings from pre-trained pLMs for downstream tasks such as contact map and function prediction.

However, the TAPE benchmark (Rao et al., 2019) highlighted opportunities for innovative design and training methods beyond traditional LSTMs and Transformers. UniRep (Alley et al., 2019a), for example, employs a multiplicative LSTM (mLSTM)(Krause et al., 2016) to condense arbitrary protein sequences into fixed-length vectors, capturing long-range dependencies. Similarly, UDSMProt(Strodthoff et al., 2020) and SeqVec (Heinzinger et al., 2019) utilize LSTM variants to develop rich, transferable representations. ProSE (Bepler & Berger, 2021) enhances these representations with structural supervision through residue-residue contact loss and structural similarity prediction, while CPCProt (Lu et al., 2020) leverages InfoNCE loss to maximize mutual information in protein embeddings.

ProtTrans (Elnaggar et al., 2021) trained extensive models (including T5, ELECTRA, ALBERT, XLNet, BERT, and Transformer-XL) on sequences comprising 393 billion amino acids across 5616 GPUs and one TPU Pod. ESM-1b (Rives et al., 2019) demonstrates how deep Transformers, coupled with a masking strategy, can build intricate context-aware representations. The results from ProtTrans and ESM-1b suggest that large-scale pLMs can effectively learn the grammar of proteins, even without evolutionary data. Furthermore, PMLM (He et al., 2022) enhances model performance on the TAPE contact benchmark by accounting for dependencies among masked tokens, indicative of inter-residue coevolution.

Incorporating additional data such as MSAs, functions, structures, and biological priors can enrich protein embeddings. For instance, the MSA Transformer (Rao et al., 2021) adapts Transformer LMs to handle

---

[6]https://github.com/Bitbol-Lab/ProtMamba-ssm/blob/8befff756b2db7b6dc56d0a07163eb02e27b2731/ProtMamba_ssm/modules.py

sets of sequences, utilizing alternating attention mechanisms. ProteinBERT (Ofer et al., 2021b) integrates sequence information with Gene Ontology (GO) annotations to predict diverse protein functions, while OntoProtein (Zhang et al., 2022) leverages GO as a factual knowledge graph. The PEER benchmarks (Xu et al., 2022) demonstrate the importance of selecting suitable auxiliary tasks to enhance model performance across a variety of protein-related tasks.

Protein Structure Prediction Early pLMs (Klausen et al., 2018; Heffernan et al., 2018; Asgari et al., 2019) primarily predicted structural features, which are essential for constructing 3D protein structures. Recent models aim to predict protein structures end-to-end. Evoformer, a core module in the AF2 network (Jumper et al., 2021), exemplifies this with its sophisticated design that includes axial attention and updates to pair representations ensuring consistency principles like the triangle inequality.

Other Applications ProGen (Madani et al., 2020) exemplifies models trained on sequences conditioned on specific protein properties. In contrast, newer models like ProGen2 (Nijkamp et al., 2022) and AminoBERT (Chowdhury et al., 2022) illustrate the expansion of pLM applications to include tasks like antibody structure prediction, demonstrating the versatile utility of pLMs across a range of biological research and clinical applications.

Appendix C   Datasets, Tasks, and Metrics

C.1   Protein Sequence Datasets

We first describe the `Unified Reference Protein (UniRef)` dataset(Suzek et al., 2015), which provides clustered sets of protein sequences from the UniProt Knowledgebase (UniProtKB) (Boutet et al., 2016) and selected UniParc records. It's designed to speed up protein sequence analysis by reducing the redundancy of sequences at different levels without losing the coverage of sequence space. Here are the key features of the `UniRef` dataset:

- `UniRef100`: This dataset includes all the protein sequences from UniProtKB and selected UniParc records, clustered by exact sequence matches. It provides comprehensive coverage and serves as the basis for the other two datasets.

- `UniRef90`: This set clusters sequences that have at least 90% sequence identity and 80% overlap in alignment, compressing the dataset while still preserving most of the sequence diversity. It is used for high-throughput and large-scale analysis where a balance between speed and coverage is needed.

- `UniRef50`: This dataset clusters sequences with at least 50% sequence identity and 80% overlap in alignment, further reducing the dataset size and redundancy. It's intended for rapid scans and for exploring broad phylogenetic relationships.

Each entry in a UniRef dataset represents a cluster and contains the sequence of the representative protein (the longest sequence or the one with the most annotations), along with a list of all the cluster members. These datasets are useful for various bioinformatics tasks such as sequence alignment, phylogenetic analysis, and functional annotation, as they allow researchers to handle large volumes of sequence data more efficiently.

We use the 2024-01 release of UniRef[7], and preprocessed by removing de-novo designed proteins by filtering out protein sequences annotated by `Tax=synthetic construct`. Next, we randomly sample 250,000 sequences from `UniRef90` as the validation set to report evaluation losses for pretraining protein language models (pLMs). To remove sequences from training sets (`UniRef50` and `UniRef90`) that are highly similar to the validation set, we use the training sets as query databases and validation set as a target database by mmseqs2 (Steinegger & Söding, 2017) with the following command: `mmseqs search -min-seq-id 0.5 -alignment-mode 3 -max-seqs 300 -s 7 -c 0.8 -cov-mode 0`.

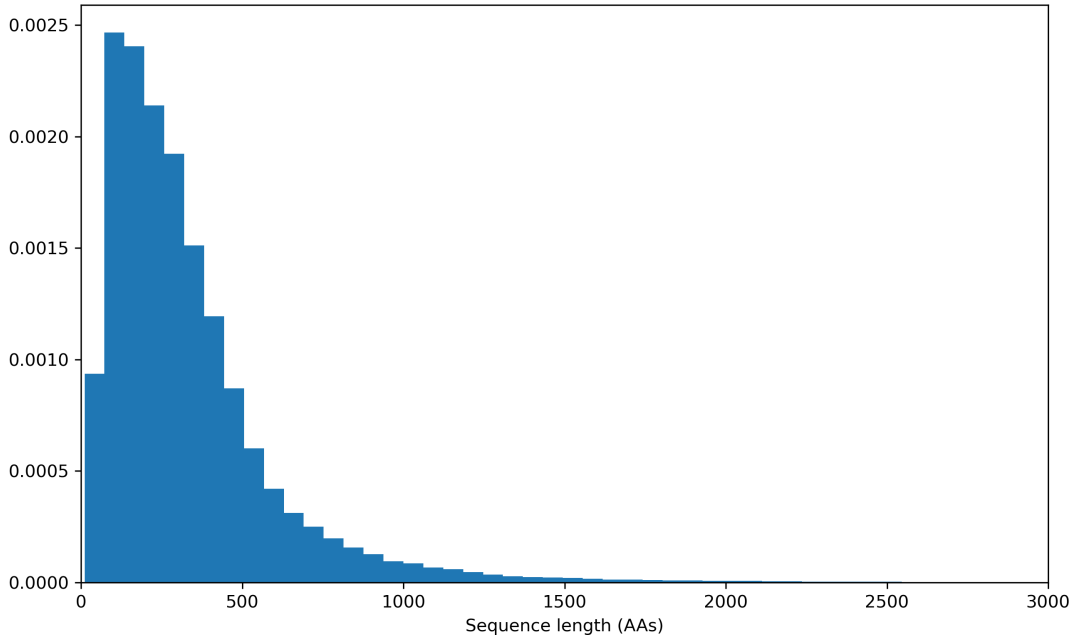[7] https://ftp.uniprot.org/pub/databases/uniprot/previous_releases/release-2024_01/uniref/

Figure 8: The sequence length distribution of `UniRef90`.

For the first-stage training of `LC-PLM` and ESM-2 models, we use the `UniRef50` training set; and for the scaling law and length extrapolation experiments, we use the `UniRef90` set. We also provide the histogram of `UniRef90` in terms of sequence length in Figure 8. The training and evaluation sets are randomly sampled from the entire set, which should follow the same distribution. The average lengths of `UniRef90` and `UniRef50` are shown in Table 5

Database	Tokens	Num sequences	Average length
UniParc	221.7B	577.8M	383.6bp
UniRef100	144.3B	376.6M	383.2bp
UniRef90	61.2B	179.5M	341.2bp
UniRef50	17.8B	62.8M	284.4bp

Table 5: Average length of `UniRef`.

C.2 Structure Prediction Datasets

`CASP15-multimers` is a subset derived from the 15th edition of Critical Assessment of Protein Structure Prediction (CASP) challenge (Kryshtafovych et al., 2023), specifically focusing on predicting the structures of protein complexes or multimers. In `CASP15`, the multimer track evaluates the ability of protein structure prediction methods to accurately model the quaternary structures of protein assemblies. `CASP15-multimers` includes 52 protein complexes.

`CASP14` is a dataset from the 14th edition of the CASP challenge (Kryshtafovych et al., 2021). CASP is a biennial experiment that assesses the state-of-the-art methods for protein structure prediction. `CASP14` covers a wide range of protein structure prediction tasks, including free modeling (FM), template-based modeling (TBM), and the prediction of protein domains with challenging folds. `CASP14` includes 37 protein structures.

`Benchmark2` (Ghani et al., 2021) is a dataset commonly used in the field of protein-protein docking and structure prediction. It is a curated collection of protein complexes that have been used extensively to evaluate the performance of computational methods in predicting the binding orientation of protein complexes. The dataset includes both bound and unbound forms of protein structures, providing a challenging testbed for docking algorithms. `Benchmark2` includes 17 heterodimers structures.

Metrics (i) `Frame Aligned Point Error (FAPE)` measures the error in aligning one set of points (predicted) to another (target), considering both translational and rotational components. The error is calculated on a per-point basis between corresponding points in the two sets, after aligning them using a frame of reference. The error is normalized by the size of the objects involved, which allows it to be invariant to the absolute size of the objects, making it suitable for tasks involving objects of varying scales. The loss is usually computed as an L1 or L2 norm of the differences in the aligned coordinates, which provides a straightforward gradient for optimization. (ii) `Distogram Loss` aims to improve the separability of feature distributions for different classes. It works by encouraging the histograms (or distributions) of distances within classes (positive pairs) to be distinct from histograms of distances between classes (negative pairs). The loss function is designed to increase the overlap between histograms of positive pairs while decreasing the overlap for negative pairs. This is achieved by calculating the probability of a randomly chosen positive pair having a smaller distance than a randomly chosen negative pair. Typically, a differentiable approximation of the histogram is used, and the optimization focuses on adjusting the model parameters to achieve the desired separation in the histograms' distributions. (iii) `pTM score` is used to assess the structural similarity between two proteins, normalized for protein size. TM scores range from 0 to 1, where a score higher than 0.5 generally indicates a model of correct topology and a score below 0.17 suggests random similarities. TM-score is more sensitive to the global fold of a protein than to the specific atomic positions, making it particularly useful in assessing larger, domain-level accuracies. (iv) `LDDT` is a local superposition-free score that evaluates the local accuracy of a protein model by comparing distances between all atom pairs within defined cutoffs in both the predicted and reference models. It can provide a more detailed view of the quality of a pLM at the residue level.

C.3 TAPE and ProteinGym

Tasks Assessing Protein Embeddings (TAPE) TAPE (Rao et al., 2019) is a set of five biologically relevant semi-supervised learning tasks spread across different domains of protein biology. We adopted four tasks: 1) Secondary Structure prediction, and 2) Remote Homology Detection, 3) Stability prediction, 4) Fluorescence prediction. Secondary structure prediction is a sequence-to-sequence task where each input amino acid is mapped to one of the three labels from {Helix, Strand, Other}. It probes the model's ability to learn local structure. Remote Homology Detection is a sequence classification task where each input protein is mapped to a label $\{1, \cdots, 1195\}$, representing different possible protein folds. This task measures models' capability to detect structural similarity across distantly related proteins. Stability and Fluorescence predictions are sequence-level regression tasks that probe the model's ability to predict the mutant sequences' properties, which are the thermostability and the flurescent intensity, respectively.

ProteinGym ProteinGym (Notin et al., 2024) is collection of benchmarks aiming at comparing the ability of models to predict the effects of protein mutations. We use the DMS Substitution subset from ProteinGym, which covers 2.5 million mutants from across 217 assays.

C.4 Datasets for Protein Function Prediction and Link Prediction on PPI Graph

ogbn-proteins The `ogbn-proteins` dataset is structured as an undirected, weighted graph with nodes and edges categorized by species. Nodes in this graph represent proteins, while the edges denote various biologically significant associations such as physical interactions, co-expression, or homology (Szklarczyk et al., 2019). Each edge is associated with an 8-dimensional feature vector, where each dimension quantifies the confidence level of a particular association type on a scale from 0 to 1—with higher values indicating greater confidence. The dataset includes proteins from eight different species. The objective is to predict protein functions using a multi-label binary classification approach, where there are 112 different functions to predict.

The performance metric used is the average ROC-AUC score across these 112 prediction tasks. The dataset is divided into training, validation, and test sets based on the species of the proteins. This split strategy is designed to assess how well models can generalize across different species. Notably, the `ogbn-proteins` dataset lacks specific input features for nodes but includes features for over 30 million edges. In baseline experiments, a simple approach is taken where the node features are derived by averaging the features of incoming edges to each node.

ogbl-ppa The `ogbl-ppa` dataset is an undirected, unweighted graph where nodes represent proteins from 58 different species, and edges illustrate biologically significant relationships between proteins, including physical interactions, co-expression, homology, or genomic neighborhood (Szklarczyk et al., 2019). Each node is described by a 58-dimensional one-hot vector indicating the species of the protein. The objective is to predict potential new association edges based on the provided training edges. The model's performance is evaluated on its ability to prioritize positive test edges over negative ones. Each positive edge in the validation or test set is ranked against 3,000,000 randomly selected negative edges. The effectiveness of the model is measured using the Hits@K metric, where K = 100 is determined to be an effective threshold in initial experiments. This metric, which requires the model to consistently rank positive edges above a vast majority of negative edges, poses a greater challenge than the ROC-AUC metric. The dataset divides edges into training, validation, and test sets based on the method used to determine the associations. Training edges consist of associations identified either through high-throughput methods (such as automated, large-scale experiments) or computationally (e.g., through text mining). Conversely, validation and test edges are derived from protein associations verified through low-throughput, labor-intensive experiments in the lab (Macarron et al., 2011; Bajorath, 2002; Younger et al., 2017). The primary challenge is to predict specific types of protein associations, like physical protein-protein interactions, based on other more readily measurable types of associations that are correlated with the target interactions.

Name	#Nodes	#Edges	Split	Task	Metric
ogbn-proteins	132,534	39,561,252	Species	Binary classification	ROC-AUC
ogbl-ppa	576,289	30,326,273	Throughput	Link prediction	Hits@100

Table 6: Summary of OGB datasets.

Appendix D Experimental Setup

D.1 Hardware and Software

All experiments are run on NVIDIA A100 Tensor Core GPU except `ogbn-proteins` and `ogbl-ppa`, which are run on NVIDIA A10G Tensor Core GPUs. For core software packages in main experiments, we use Python 3.10, PyTorch 2.1.0, Transformers 4.41.2, DeepSpeed 0.14.4, Accelerate 0.27.2, mamba-ssm 2.2.0, datasets 2.20.0, Triton 2.0.0, and CUDA Toolkit 12.1. For some downstream tasks, the dependencies and package version will be adjusted accordingly. For `ogbn-proteins` and `ogbl-ppa`, we add several new packages: PyTorch Geometric 2.5.3, torch-cluster 1.6.3, torch-scatter 2.1.2, torch-sparse 0.6.18, torch-spline-conv 1.2.2, and OGB 1.3.6.

D.2 Masked Language Modeling

The input to the model consists of raw protein sequences, which are tokenized into individual amino acids. A subset of these amino acids is randomly selected and masked during training. Typically, 15% of the amino acids in a sequence are selected for masking. Of these selected tokens, 80% are replaced with a special [MASK] token, 10% are replaced with a random amino acid, and the remaining 10% are left unchanged. The model is trained to predict the identity of these masked amino acids using a cross-entropy loss.

The training process is conducted using the AdamW optimizer with a learning rate that is linearly warmed up for a small percentage of the total training steps, followed by a cosine decay schedule. The batch size and

learning rate are chosen based on the model size and computational resources, with a total number of tokens approximately equal to $0.5M$[8] and learning rates are set as 2×10^{-4}. Gradient clipping is often applied to stabilize the training. Additionally, a 0.1 weight decay is applied.

For second-phase training with graph context, we sample random walks with the context length $l = 5$ on the given PPI graph (`ogbn-proteins` or `ogbl-ppa`) and retrieve the corresponding protein sequence for each node from String database (Szklarczyk et al., 2019). We then add 4 special tokens to indicate the begin and end of the node, the edge and non-edge in the random walk path. We continue MLM training the 740M `LC-PLM` on 20B more tokens on random walks to get `LC-PLM-G`, during which we freeze the parameters in SSMs and linear projection layers except the input & output embeddings and normalization layers. We summarize the key hyperparameters in table 7.

D.3 Structure Prediction with LMFold

To train LMFold, we use the FAPE and distogram losses introduced in AlphaFold2 (Jumper et al., 2021), as well as heads for predicting LDDT and the pTM score. We weigh these 4 loss terms using the default constants proposed in OpenFold (Ahdritz et al., 2024). We used Adam with $\beta_1 = 0.9$, $\beta_2 = 0.99$, and $\epsilon = 1^{-6}$ as optimizers, and warmed up the learning rate linearly over the first 1,000 iterations from 0 to 1^{-3}. We use a per-GPU batch size of 1 training on 32 NVIDIA A100 GPUs, leading to a global batch size of 32.

Hyperparameters	100M	340M	740M	1.3B
Peak learning rate	2×10^{-4}			
Global batch size	0.5M tokens			
Block size	1024			
Warm-up steps	2000			
Adam betas	$\beta_1 = 0.9, \beta_2 = 0.95$			
Maximum gradient norm	0.5			
Precision	BF16			
Optimizer	AdamW			
Learning rate scheduler	cosine			
Weight decay	0.1			
Length of random walks	5			
Hidden size	768	1024	1536	2048
Number of `BiMamba-S` blocks	24	48	48	48

Table 7: Summary of MLM training hyperparameters for `LC-PLM` and `LC-PLM-G`.

D.4 Evaluation on TAPE tasks

To evaluate pretrained pLMs on TAPE Remote Homology prediction and Secondary Structure prediction, we followed the evaluation setting from Rao et al. (2019). For the Remote Homology task, we add a two-layered MLP (with 512 as the intermediate dimension) on top of the protein-level embeddings from a pLM. The protein-level embeddings are calculated as the average of token-level embeddings. For the Secondary Structure prediction task, we used a single-layered MLP taking the token-level embeddings from the LM directly to make a token-level 3-class classification.

Then, we fine-tune the parameters of the LM and the MLP prediction head end-to-end on the training set and perform early stopping on the validation set. We report the top-1 accuracy on the fold-level hold-out test set for Remote Homology task, accuracy on the CB513 test set for the Secondary Structure prediction task, and spearman's rho on Stability prediction task, respectively. The detailed hyperparameters we used are listed in Table 9.

---

[8]For 100M, 340M, 740M, and 1.3B of `LC-PLM`, we train on 16, 32, 64, 128 A100s, respectively. The local batch size and the gradient accumulation steps are dynamically adjusted to ensure the model fits in.

Hyperparameters	150M	300M	650M	1.0B
Peak learning rate		2×10^{-4}		
Global batch size		0.5M tokens		
Warm-up steps		2000		
Adam betas		$\beta_1 = 0.9, \beta_2 = 0.98$		
Maximum gradient norm		1.0		
Precision		BF16		
Optimizer		AdamW		
Learning rate scheduler		cosine		
Weight decay		0.01		
Length of random walks		5		
Hidden size	640	960	1280	1280
Intermediate size	2560	3840	5120	7680
Number of hidden layers	30	30	33	33

Table 8: Summary of MLM training hyperparameters for ESM-2.

Hyperparameters	Remote Homology	Secondary Structure	Stability
Batch size		16	512
Number of warm-up steps		5000	
Early stopping patience		25 epochs	
Max number of epochs		100	
Learning rate decay schedule		cosine	
Optimizer		AdamW	
Adam betas		$\beta_1 = 0.9, \beta_2 = 0.98$	
Peak learning rate	1e-5	5e-5	1e-4
Prediction head	2-layered MLP	1-layered MLP	2-layered MLP

Table 9: Hyperparameters used for fine-tuning protein language models for TAPE tasks.

D.5 Evaluating on ProteinGym

To evaluate pretrained pLMs on the ProteinGym DMS Substitution benchmarks, we adopt the masked-marginals heuristic (Meier et al., 2021) to predict protein fitness in a zero-shot setting. The masked-marginals method scores mutations (mt) using the log odds ratio at the mutated position over wild-type (wt), assuming an additive model when multiple mutations T exist in the same protein sequence:

$$\sum_{t \in T} \log p(x_t = x_t^{mt} | x_{\setminus T}) - \log p(x_t = x_t^{wt} | x_{\setminus T})$$

We then compute Spearman's correlation coefficient and normalized discounted cumulative gain (NDCG) between the log odds ratio and the experimentally measured protein fitness scores for each DMS assay. The Spearman's correlation coefficients are aggregated across 217 DMS assays using the provided code.

D.6 Protein Function Prediction and PPI Link Prediction

For protein function prediction on `ogbn-proteins`, we use GIPA (Li et al., 2023) as the graph neural network (GNN) backbone with our learned protein sequence embeddings as the node attributes initialization. We report the hyperparameters (HPs) we use to train the model in Table 10. Furthermore, we conduct more ablation studies on the GNN backbone to test if the contribution of learned protein embeddings is independent of the architecture design choice. We choose two popular GNNs, i.e. GCN (Kipf & Welling, 2017) and GraphSAGE (Hamilton et al., 2017) to evaluate the embeddings. The HPs are shown in Table 11.

For PPI link prediction on `ogbl-ppa`, we use a combined backbone of NGNN (Song et al., 2021) and SEAL (Zhang & Chen, 2018) with labeling tricks (Zhang et al., 2021). We summarize the HPs used in this backbone in Table 12. Note that there is a ratio k used in SortPooling (Zhang et al., 2018). We also perform similar ablation studies on this task using GCN and GraphSAGE with the same set of HPs reported in Table 11.

Hyperparameters	Value
# of epochs	1500
# of heads	20
Learning rate	0.01
# of layers	6
# of hidden units	50
Dropout rate	0.4

Table 10: HPs of GIPA backbone.

Hyperparameters	Value
# of epochs	1000
# of heads	20
Learning rate	0.01
# of layers	3
# of hidden units	256
Dropout rate	0.3

Table 11: HPs of GCN/SAGE.

Hyperparameters	Value
# of epochs	50
k of SortPooling	0.6
Learning rate	0.00015
# of layers	3
# of hidden units	48
Dropout rate	0.0

Table 12: HPs of NGNN/SEAL.

Appendix E   More results and details on TAPE

For the Jacobian contact map prediction task we reported in the main paper, we adopted the methods from Zhang et al. (2024b) to use categorical Jacobian matrices computed from protein language models as the zero-shot prediction for protein contact maps and report the precision@2/L (L is the length of a protein sequence) on the validation set of ProteinNet dataset (AlQuraishi, 2019).

Model (#Tokens trained)	PPI graph	Fluorescence
ESM-2-650M (100B)	None	0.695 ± 0.002
ESM-2-G-650M (100B)	ogbn-proteins	0.694 ± 0.002
ESM-2-G-650M (100B)	ogbl-ppa	0.693 ± 0.001
`LC-PLM`-740M (100B)	None	0.692 ± 0.002
`LC-PLM-G`-740M (100B)	ogbn-proteins	0.709 ± 0.003
`LC-PLM-G`-740M (100B)	ogbl-ppa	0.693 ± 0.002
ProtMamba-public	None	0.688 ± 0.005
CARP-640M-public	None	0.680 ± 0.002
ESM-2-650M-public (1T)	None	0.688 ± 0.001
`LC-PLM-G`-740M (100B)	ogbl-ppa	0.691 ± 0.003

Table 13: Evaluation on TAPE tasks in supervised fine-tuning setting. We report the Spearman's correlation coefficients for the test sets for Fluorescence prediction tasks. We perform 3 runs using different seeds to report the mean and standard deviation.

Appendix F   More results on ProteinGym

We report more results and comparisons on ProteinGym with some other baselines, i.e. PoET (Truong Jr & Bepler, 2023), TranceptEVE-L (Notin et al., 2022), and SaProt (Su et al., 2023), which use additional information like structural tokens.

The results demonstrate that `LC-PLM` performs better with less training tokens, as shown in Table 4; however, with sufficient training tokens, ESM2 can achieve comparable or even better performance on this task, as shown in Table 14. The sequence-only methods like ESM2 and `LC-PLM` have lower numbers than the other baselines, showing that structure information is useful for ProteinGym DMS substitutions.

Model (#Tokens trained)	PPI graph	Spearman	NDCG
ESM-2-650M-public (1T)	None	0.414 ± 0.011	0.747 ± 0.005
ESM-2-3B-public (1T)	None	0.406 ± 0.011	0.755 ± 0.004
`LC-PLM`-740M (1T)	None	0.388 ± 0.009	0.751 ± 0.004
PoET (Truong Jr & Bepler, 2023)	None	0.479	N/A
TranceptEVE-L (Notin et al., 2022)	None	0.454	0.786
SaProt (Su et al., 2023)	None	0.457	0.768

Table 14: Evaluation on ProteinGym DMS substitutions benchmark. We report *Spearman's correlation coefficient* and *normalized discounted cumulative gain (NDCG)* between the log odds ratio and the experimentally measured protein fitness scores for each DMS assay.

Appendix G Robustness of downsampling for structure prediction training set

We perform three 1.5% downsampling using three random seeds and retrain both our LC-PLM and ESM-2. We find that the downsampling is very robust to the performance with a small standard deviation that is close to (even smaller than) the standard deviation of using the same train set but training with different random seeds as we reported in Table 15.

Model (#Tokens trained)	CASP15-multimers	CASP14	Benchmark2
ESM-2-650M (100B)	0.4132 ± 0.0065	0.3437 ± 0.0039	0.4773 ± 0.0092
`LC-PLM`-740M (100B)	0.5004 ± 0.0139	0.4244 ± 0.0053	0.6290 ± 0.0121
ESM-2-650M-public (1T)	0.5128 ± 0.0003	0.4421 ± 0.0023	0.6844 ± 0.0059

Table 15: Structure prediction performance (*TM score*) on `CASP15-multimers`, `CASP14`, and `Benchmark2`. We perform 3 downsamplings using different seeds and report the mean and standard deviation.

Appendix H More Details for Protein Function Prediction and PPI Link Prediction

We evaluate `LC-PLM-G`'s performance on two graph-related downstream tasks, protein structure prediction and PPI link prediction on OGB (Hu et al., 2020), i.e. `ogbn-proteins` and `ogbl-ppa`. Both datasets provide a PPI graph but with different scales (i.e. the numbers of nodes and edges) and predict different tasks (i.e. node property prediction and link prediction). Given the benefit of our graph-contextual training, we have a more principled way to obtain the protein representations from `LC-PLM-G` or ESM-2-G by averaging the embeddings of `[BON]` and `[EON]` (Note that to impose the inductive bias of the learned distribution of positive random walk paths to the embedding, we concat an `[EDGE]` token right after `[EON]` such that the output embeddings will be pulled towards the positive, i.e. existing graph context). In contrast, we can only obtain the protein embeddings from ESM-2 or `LC-PLM` by averaging the AA token embeddings, which are not very informative. We show the evaluation results on `ogbn-proteins` in Table 16 against a set of popular baselines. Our model achieves the best demonstration of the benefits of having graph context-aware protein embeddings learned in `LC-PLM-G`. We also provide ablation studies in Tables 17 and 18 where we choose two GNN backbones GCN and GraphSAGE to evaluate if the learned embeddings from `LC-PLM` and `LC-PLM-G` are beneficial to this task. The evidence shows that the learned embeddings consistently improve the performance and the graph context provides another boost.

As discussed in Section 6, we can also perform more graph-specific self-supervised learning (Wang et al., 2021b;c;a; Zhao et al., 2022) within the given graph context before supervised fine-tuning. By using this, we may obtain better initialization for node embeddings which would potentially encode the graph context better and improve the final prediction performance.

Model	Accuracy
Node2vec (Grover & Leskovec, 2016)	0.6881 ± 0.0065
GCN (Kipf & Welling, 2017)	0.7251 ± 0.0035
GraphSAGE (Hamilton et al., 2017)	0.7443 ± 0.0064
DeepGCN (Li et al., 2019)	0.8496 ± 0.0028
GAT (Veličković et al., 2017)	0.8501 ± 0.0046
DeeperGCN (Li et al., 2020)	0.8580 ± 0.0017
UniMP (Shi et al., 2020)	0.8642 ± 0.0008
GIPA (Li et al., 2023)	0.8700 ± 0.0010
ESM-2-G	0.8920 ± 0.0008
`LC-PLM-G`	**0.8925 ± 0.0010**

Table 16: Performance on `ogbn-proteins`.

Model	Accuracy
GCN	0.7251 ± 0.0035
GCN+`LC-PLM`	0.7643 ± 0.0042
GCN+`LC-PLM-G`	**0.7668 ± 0.0056**
GraphSAGE	0.7443 ± 0.0064
GraphSAGE + `LC-PLM`	0.7662 ± 0.0021
GraphSAGE + `LC-PLM-G`	**0.7679 ± 0.0029**

Table 17: Ablations on `ogbn-proteins`.

Model	Hits@100
GCN	0.1867 ± 0.0132
GCN+`LC-PLM`	0.1946 ± 0.0142
GCN+`LC-PLM-G`	**0.1988 ± 0.0156**
GraphSAGE	0.1655 ± 0.0240
GraphSAGE + `LC-PLM`	0.1847 ± 0.0193
GraphSAGE + `LC-PLM-G`	**0.1876 ± 0.0164**

Table 18: Ablations on `ogbl-ppa`.

Appendix I   On the Absence of Massive Activations

Recent studies (Sun et al., 2024) have highlighted the phenomenon of massive activations in Transformer-based models, particularly large language models (LLMs) such as LLaMA2 and GPT-2. These massive activations refer to a small number of hidden units exhibiting values that are several orders of magnitude larger than the median activation—often input-agnostic and acting as implicit bias terms throughout the model. This behavior, while seemingly innocuous, introduces challenges in quantization and numerical stability, and can negatively affect interpretability and robustness.

To examine whether this issue extends to protein language models, we analyzed internal activations in ESM2 (650M) and `LC-PLM` (740M). Unlike ESM2, which clearly exhibits massive activations in intermediate layers (with magnitudes exceeding 400 in some layers), `LC-PLM` do not exhibit any such spikes in activation magnitude across layers (Figure 9). Across all layers, the largest BiMamba activations remain within a modest range, closely tracking the median.

This absence of massive activations in `LC-PLM` has some implications: (1) Improved numerical stability: Lower variance in activation magnitudes reduces the risk of gradient explosion or instability during fine-tuning or continued pretraining; (2) Quantization-friendly: Models without large outlier activations are significantly easier to quantize using standard techniques, potentially allowing for more aggressive compression without accuracy loss. While the exact architectural mechanisms underlying the absence of massive activations in `LC-PLM` remain to be fully understood, we hypothesize that the recurrent state-space structure of Mamba layers inherently mitigates the formation of such activations.

Appendix J   Pseudocode

We provide a detailed breakdown of our algorithm in this section and then we summarize this computation procedure into a pseudocode algorithmic block as shown in Algorithm 1. The algorithm procedure can be stated as follows:
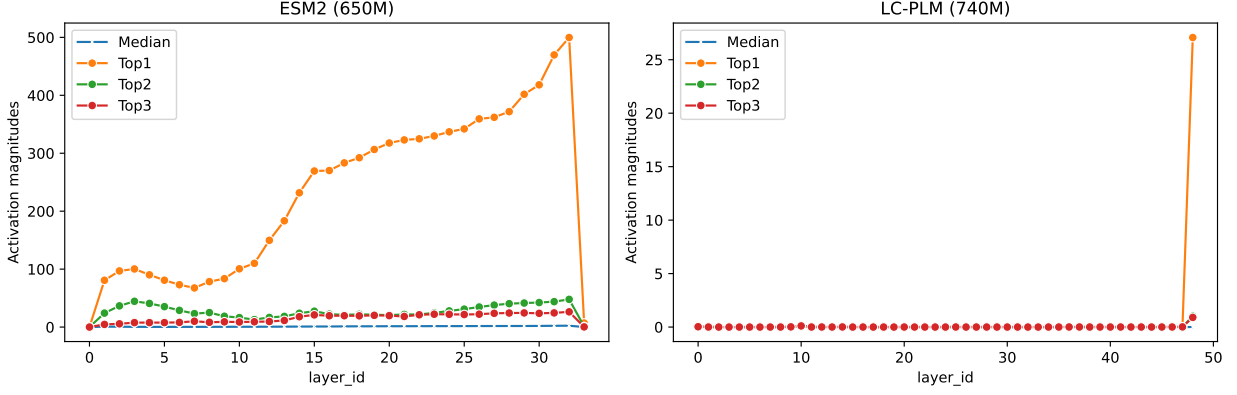
Figure 9: Activation magnitude of intermediate layers in ESM2 and `LC-PLM`.

Input $\mathbf{T}_{l-1} : (B, S, D)$ tensor, where B is batch size, S is sequence length, and D is hidden state dimension.

Output $\mathbf{T}_l : (B, S, D)$ tensor.

Process 1. Normalization $\mathbf{T}'_{l-1} : (B, S, D) \leftarrow \text{Norm}(\mathbf{T}_{l-1})$

      2. Reversal $\hat{\mathbf{T}}'_{l-1} : (B, S, D) \leftarrow \text{Reverse}\left(\mathbf{T}'_{l-1}\right)$

      3. Parallel Processing For both $\mathbf{T}'_{l-1}$ and $\hat{\mathbf{T}}'_{l-1}$, denoted as $\mathbf{T}'_{*,l-1}$:

          a. Linear Transformations

$$\mathbf{X}_{*,l-1} : (B, S, E) \leftarrow \text{Linear}^{\mathbf{X}_{*,l-1}}(\mathbf{T}'_{*,l-1})$$
$$\mathbf{Z}_{*,l-1} : (B, S, E) \leftarrow \text{Linear}^{\mathbf{Z}_{*,l-1}}(\mathbf{T}'_{*,l-1})$$

          b. Convolution and Activation $\mathbf{X}'_{*,l-1} : (B, S, E) \leftarrow \text{SiLU}(\text{Conv1d}(\mathbf{X}_{*,l-1}))$

          c. Additional Linear Transformations

$$\mathbf{B}_{*,l-1} : (B, S, N) \leftarrow \text{Linear}^B_{*,l-1}(\mathbf{X}'_{*,l-1})$$
$$\mathbf{C}_{*,l-1} : (B, S, N) \leftarrow \text{Linear}^C_{*,l-1}(\mathbf{X}'_{*,l-1})$$

          d. Delta Computation

$$\Delta_{*,l-1} : (B, S, E) \leftarrow \log(1 + \exp(\text{Linear}^{\Delta}_{*,l-1}(\mathbf{X}'_{*,l-1}) + \text{Parameter}^{\Delta}_{*,l-1}))$$

          e. Parameter Scaling $\bar{\mathbf{A}}_{*,l-1} : (B, S, E, N) \leftarrow \Delta_{*,l-1} \otimes \text{Parameter}^{\bar{A}}_{*,l-1}$

          f. B Update $\mathbf{B}_{*,l-1} : (B, S, E, N) \leftarrow \Delta_{*,l-1} \otimes \mathbf{B}_{*,l-1}$

          g. State Space Model Application

$$\mathbf{Y}_{*,l-1} : (B, S, E) \leftarrow \text{SSM}(\bar{\mathbf{A}}_{*,l-1}, \mathbf{B}_{*,l-1}, \mathbf{C}_{*,l-1})(\mathbf{X}'_{*,l-1})$$

          h. Final Computation $\mathbf{Y}'_{*,l-1} : (B, S, E) \leftarrow \mathbf{Y}_{*,l-1} \odot \text{SiLU}(\mathbf{Z}_{*,l-1})$

      4. Combination and Output $\mathbf{T}_l : (B, S, D) \leftarrow \text{Linear}^T(\mathbf{Y}'_{l-1} + \hat{\mathbf{Y}}'_{l-1}) + \mathbf{T}_{l-1}$

Key Operations Norm Normalization operation

      Linear Linear transformation

      Conv1d 1D Convolution

      SiLU Sigmoid Linear Unit activation function

      SSM State Space Model

      $\otimes$ Element-wise multiplication

      $\odot$ Element-wise multiplication

Algorithm 1 `BiMamba-S` Block

Input: $\mathbf{T}_{l-1} : (B, S, D)$
Output: $\mathbf{T}_l : (B, S, D)$

1: $\mathbf{T}'_{l-1} : (B, S, D) \leftarrow \text{Norm}(\mathbf{T}_{l-1})$
2: $\hat{\mathbf{T}}'_{l-1} : (B, S, D) \leftarrow \text{Reverse}\left(\mathbf{T}'_{l-1}\right)$
3: **for** $\mathbf{T}'_{*,l-1} \in \{\mathbf{T}'_{l-1}, \hat{\mathbf{T}}'_{l-1}\}$ **do**
4:     $\mathbf{X}_{*,l-1} : (B, S, E) \leftarrow \text{Linear}^{\mathbf{X}_{*,l-1}}(\mathbf{T}'_{*,l-1})$
5:     $\mathbf{Z}_{*,l-1} : (B, S, E) \leftarrow \text{Linear}^{\mathbf{Z}_{*,l-1}}(\mathbf{T}'_{*,l-1})$
6:     $\mathbf{X}'_{*,l-1} : (B, S, E) \leftarrow \text{SiLU}(\text{Conv1d}(\mathbf{X}_{*,l-1}))$
7:     $\mathbf{B}_{*,l-1} : (B, S, N) \leftarrow \text{Linear}^B_{*,l-1}(\mathbf{X}'_{*,l-1})$
8:     $\mathbf{C}_{*,l-1} : (B, S, N) \leftarrow \text{Linear}^C_{*,l-1}(\mathbf{X}'_{*,l-1})$
9:     $\Delta_{*,l-1} : (B, S, E) \leftarrow \log(1 + \exp(\text{Linear}^{\Delta}_{*,l-1}(\mathbf{X}'_{*,l-1}) + \text{Parameter}^{\Delta}_{*,l-1}))$
10:     $\bar{\mathbf{A}}_{*,l-1} : (B, S, E, N) \leftarrow \Delta_{*,l-1} \otimes \text{Parameter}^{\bar{A}}_{*,l-1}$
11:     $\bar{\mathbf{B}}_{*,l-1} : (B, S, E, N) \leftarrow \Delta_{*,l-1} \otimes \mathbf{B}_{*,l-1}$
12:     $\mathbf{Y}_{*,l-1} : (B, S, E) \leftarrow \text{SSM}(\bar{\mathbf{A}}_{*,l-1}, \bar{\mathbf{B}}_{*,l-1}, \mathbf{C}_{*,l-1})(\mathbf{X}'_{*,l-1})$
13:     $\mathbf{Y}'_{*,l-1} : (B, S, E) \leftarrow \mathbf{Y}_{*,l-1} \odot \text{SiLU}(\mathbf{Z}_{*,l-1})$
14: **end for**
15: $\mathbf{T}_l : (B, S, D) \leftarrow \text{Linear}^T(\mathbf{Y}'_{l-1} + \hat{\mathbf{Y}}'_{l-1}) + \mathbf{T}_{l-1}$
16: **return** $\mathbf{T}_l$

Appendix K   Sampling Bias in Random Walk

For random walk sampling, there are two parameters p and q we can use to control the direction of exploration (a balance between the depth-first search (DFS) and breath-first search (BFS)).

Return Parameter p Parameter p controls the likelihood of immediately revisiting a node. A high value ($p > \max(q, 1)$) reduces the chance of sampling an already-visited node, encouraging moderate exploration and avoiding 2-hop redundancy.

In-out Parameter q Parameter q allows the search to differentiate between "inward" and "outward" nodes:

- If $q > 1$, the walk is biased towards nodes close to node t, approximating BFS behavior.

- If $q < 1$, the walk tends to visit nodes further from node t, encouraging outward exploration similar to DFS.

Benefits over Pure BFS/DFS   Random walks offer several advantages over traditional BFS/DFS approaches:

1. **Computational Efficiency:** They are efficient in terms of both space and time requirements.

2. **Scalability:** The space complexity to explore the immediate neighbors of every node is $O(|E|)$ for a graph with edge set E.

3. **Flexibility:** For 2nd order random walks, the space complexity becomes $O(a^2|V|)$, where a is the average degree of the graph and V is the vertex set.

4. **Effective Sampling:** Random walks provide a convenient mechanism to increase the effective sampling rate by reusing samples across different source nodes.

5. **Parallel Sampling:** Due to the Markovian nature of the random walk, k samples for $l - k$ nodes can be generated at once, resulting in an effective complexity of $O(\frac{l}{k(l-k)})$ per sample.

This approach combines the benefits of BFS and DFS, allowing for a more nuanced exploration of network structures that exhibit both structural equivalence and homophily.

Appendix L   Training and Evaluation Curves

L.1   The First-stage Pretraining

We show the training and evaluation loss curves in Figure 10 for our first-stage pretraining of `LC-PLM` on 100B `UniRef50`. This pretrained model is used in all downstream task evaluations reported in the paper.
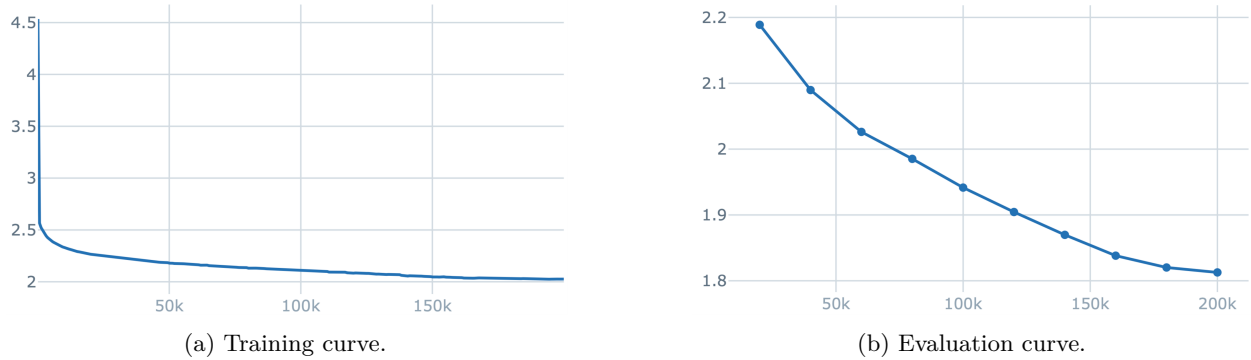

(a) Training curve.   (b) Evaluation curve.

Figure 10: The first-stage pretraining of 740M `LC-PLM` on 100B `UniRef50`. The evaluation set is 250K `UniRef90`.

L.2   The Scaling Law Experiments

We show the training and evaluation loss curves in Figure 11, Figure 12, Figure 13, and Figure 14 for our scaling law training of 100M, 340M, 740M, and 1.3B `LC-PLM` on 20B `UniRef90`. The evaluation set is the held-out 250K `UniRef90`.

(a) Training curve.   (b) Evaluation curve.
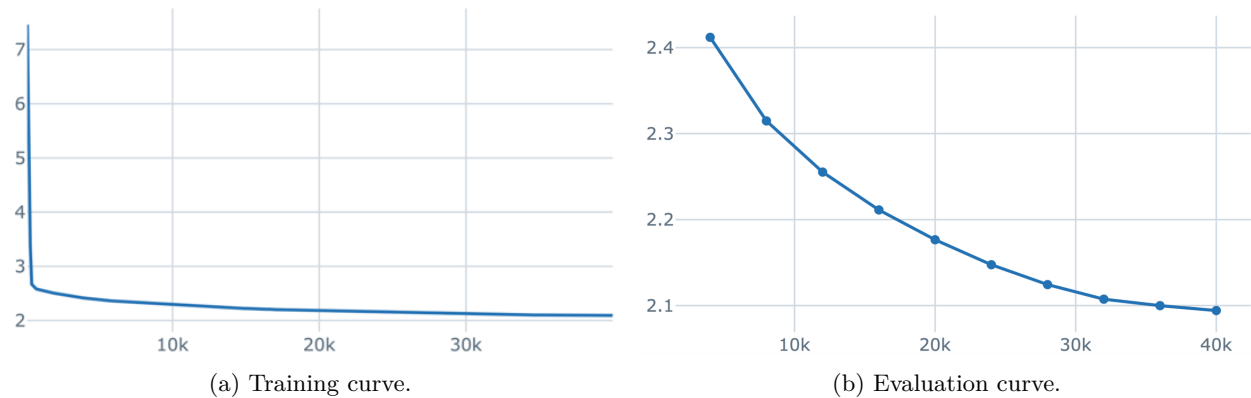
Figure 11: The scaling law training of 100M `LC-PLM` on 20B `UniRef90`. The evaluation set is 250K `UniRef90`.

L.3   The Length Extrapolation Experiments

We show the training and evaluation loss curves in Figure 15, Figure 16, and Figure 17 for our scaling law training of 100M, 340M, and 740M `LC-PLM` on the 128-256 bin of `UniRef90`. The evaluation set is the held-out 250K `UniRef90`.
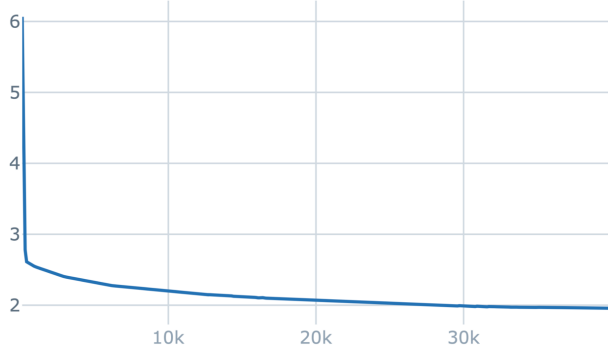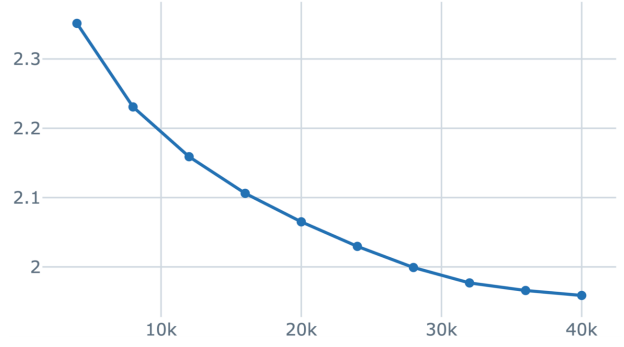
(a) Training curve.

(b) Evaluation curve.

Figure 12: The scaling law training of 340M `LC-PLM` on 20B `UniRef90`. The evaluation set is 250K `UniRef90`.
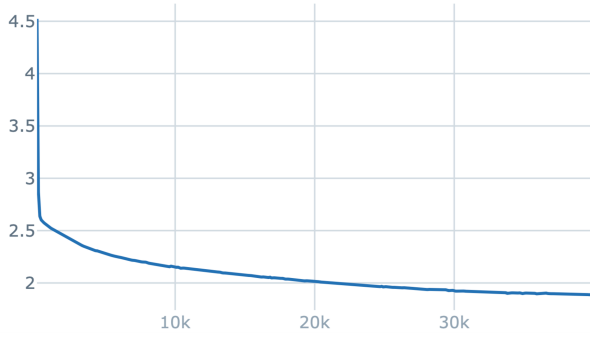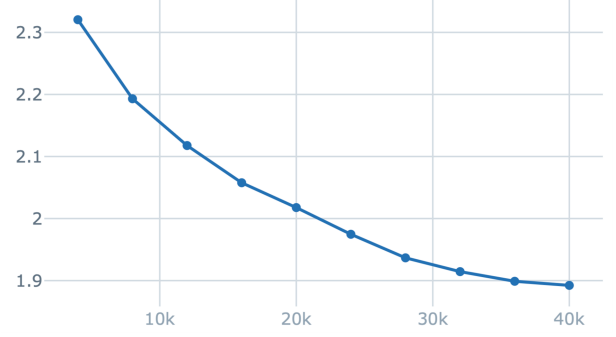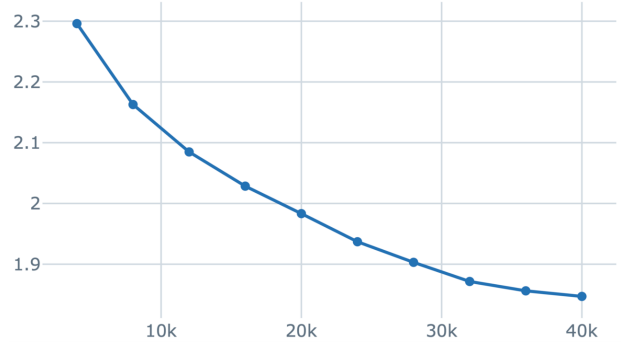

(a) Training curve.

(b) Evaluation curve.

Figure 13: The scaling law training of 740M `LC-PLM` on 20B `UniRef90`. The evaluation set is 250K `UniRef90`.
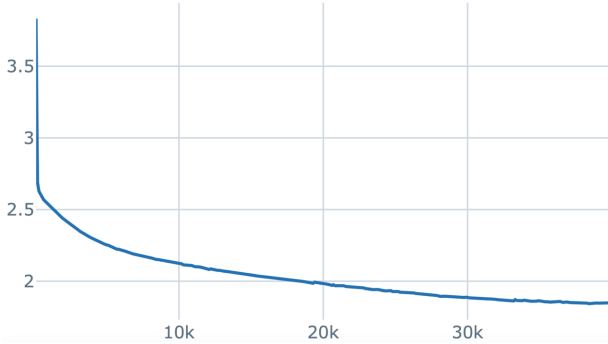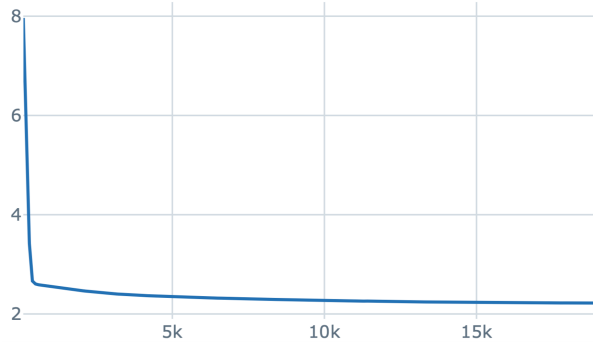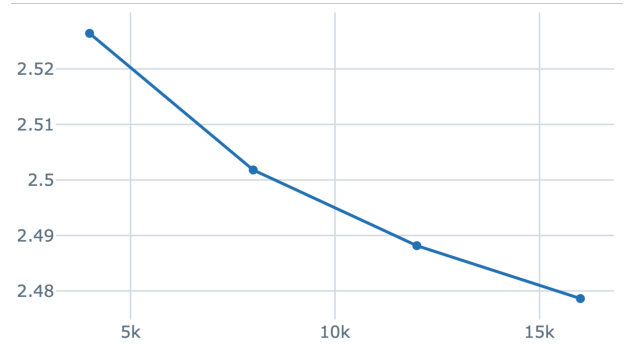

(a) Training curve.

(b) Evaluation curve.

Figure 14: The scaling law training of 1.3B `LC-PLM` on 20B `UniRef90`. The evaluation set is 250K `UniRef90`.

L.4 The Second-stage Graph Contextual Training

We show the training loss curves in Figure 18a, and Figure 18b for our second-stage graph contextual training of 740M `LC-PLM-G` on protein sequences included in `ogbn-proteins` and `ogbl-ppa`. The evaluation set is the held-out 250K `UniRef90`.

(a) Training curve.

(b) Evaluation curve.

Figure 15: The length extrapolation training of 100M `LC-PLM` on the 128-256 bin of `UniRef90`. The evaluation set is 250K `UniRef90`.
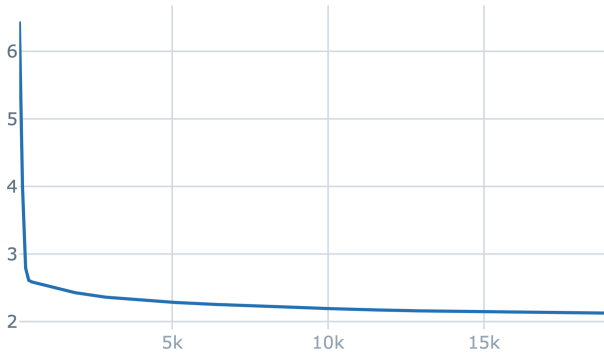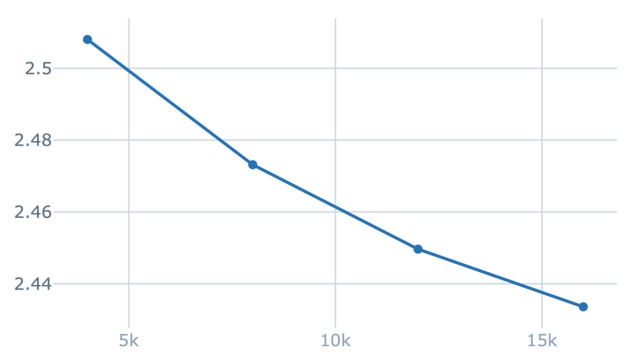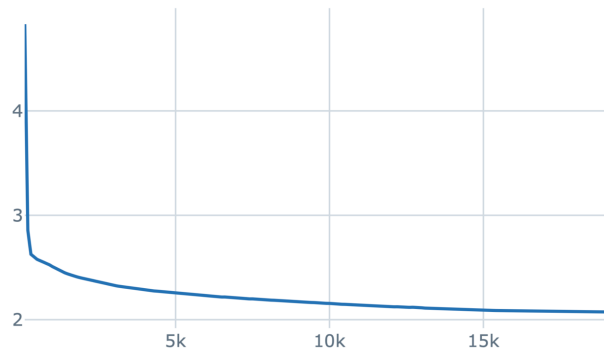

(a) Training curve.

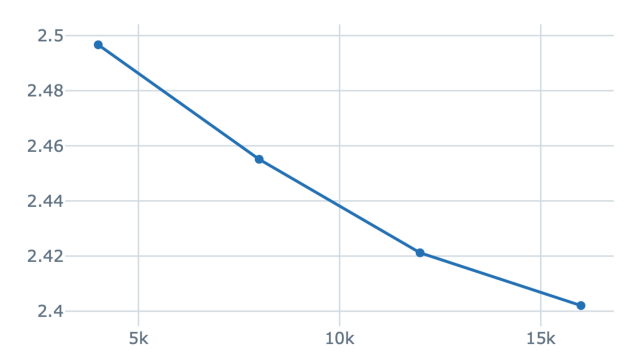

(b) Evaluation curve.

Figure 16: The length extrapolation training of 340M `LC-PLM` on the 128-256 bin of `UniRef90`. The evaluation set is 250K `UniRef90`.
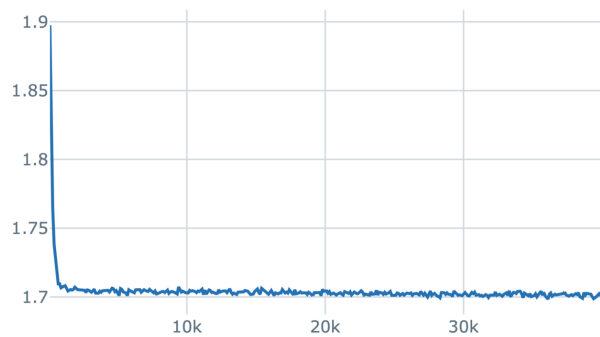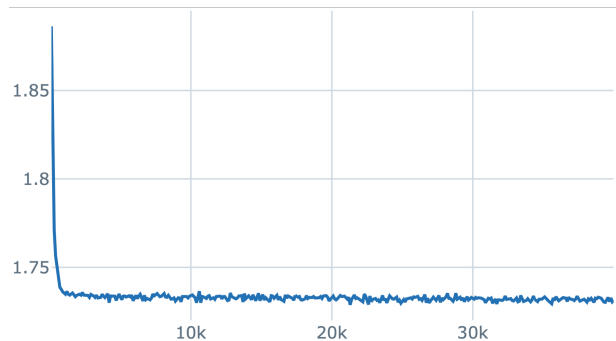

(a) Training curve.

(b) Evaluation curve.

Figure 17: The length extrapolation training of 740M `LC-PLM` on the 128-256 bin of `UniRef90`. The evaluation set is 250K `UniRef90`.

(a) Training curve on `ogbn-proteins`.

(b) Training curve on `ogbl-ppa`.

Figure 18: The second-stage training of 740M `LC-PLM-G` on `ogbn-proteins` and `ogbl-ppa`. The evaluation set is 250K `UniRef90`.